

---

## Chapter

# 14

# *Multiscale analysis: spatial eigenfunctions*

## 14.0 Introduction to multiscale analysis

Tobler's (1970) first law of geography states that "Everything is related to everything else, but near things are more related than distant things". This law is at the core of spatial analysis and modelling in geography and related fields such as biogeography, community ecology, population biology, landscape ecology and landscape genetics.

Spatial eigenfunction analysis is a family of methods for multiscale analysis of univariate or multivariate response data. Based on the theory introduced in Section 1.1 concerning the origin of spatial structures in ecosystems, these methods draw upon several developments discussed earlier in this book: distances (Chapter 7), principal coordinate analysis (Section 9.3), multiple regression modelling (Section 10.3.3), redundancy analysis (Section 11.1), variation partitioning (Sections 10.3.5 and 11.1.11), and the concept of scale in spatial patterns (Section 13.0).

The expression *spatial eigenfunction analysis* was proposed by Griffith & Peres-Neto (2006) for the whole family of methods where eigenvectors of spatial configuration matrices are computed and used as predictors in linear models, including the full range of general and generalized linear models\*. The expression proposed by these authors covers both the early methods developed by geographers to analyse binary spatial connection matrices (Garrison & Marble, 1964; Gould, 1967; Tinkler, 1972; Griffith, 1996; these methods are briefly described in Subsection 14.2.2) and the more recent methods that take into account the distances among localities and are described in the present chapter. Extension of spatial eigenfunction analysis to time series is straightforward; all methodological developments in this chapter labelled "spatial" could readily be changed to "temporal".

---

\* These two forms of linear models are described on the Web pages [http://en.wikipedia.org/wiki/General\\_linear\\_model](http://en.wikipedia.org/wiki/General_linear_model) and [http://en.wikipedia.org/wiki/Generalized\\_linear\\_model](http://en.wikipedia.org/wiki/Generalized_linear_model).

Multiscale spatial analysis is used to answer questions like the following:

- Description: What are the spatial scales of variation of the [univariate or multivariate] response data under study? What are the spatial patterns at these scales?
- Explanation (in the sense of Subsection 10.2.1): What are the processes that explain (meaning *account for*) the spatial variation of the response data at different scales? Indeed, different processes may affect (or be associated with) that spatial variation at different scales.
- For communities of organisms, beta diversity is the spatial variation in community composition among sites (Subsection 6.5.3). How does beta diversity relate to different types of processes at different scales, for example environmental control (Subsection 1.1.1, model 1) and neutral processes (Subsection 1.1.1, model 2)?

Space

In multiscale spatial analysis, the variation in response data is analysed with respect to variables (eigenfunctions) representing geographic variation, which may be divided into submodels corresponding to different spatial scales; see the following sections. Of course, space *per se* cannot be considered as an explanation of ecological variability. The spatial variables used as explanatory variables in analyses are proxies for real environmental or ecological explanatory variables. The spatial proxies serve to quantify and dissect the spatial variation present in the response data. Part of that variation can then be attributed to some of the potentially explanatory variables that are available for analysis, the remainder being considered as spatial variation that remains to be explained. Subsection 14.1.4 discusses different hypotheses that can be invoked to explain such variation.

Trend-surface analysis described in Subsection 13.2.1 and used for spatial modelling in Section 13.5 is a rather crude method. A model that simply uses the spatial coordinates is sufficient to model a flat surface; a quadratic model (coordinates to the powers 1 and 2) can represent a bowl or saddle shape; a cubic model (powers 1, 2 and 3) has one more bend in each geographic direction. To model fine structures would require a polynomial equation with more monomials than there are objects, which would render the method useless in practice for data analysis.

Given the lack of efficient methods to model multiscale spatial structures until the late 1990's and the beginning of the 21st century, researchers were then looking for appropriate approaches. Ideally, the modelling matrix should contain mutually orthogonal vectors; because of that property, these vectors could be combined into submodels, corresponding to different spatial scales, that would be linearly independent of one another in variation partitioning. The following sections describe modelling methods that meet these expectations: dbMEM analysis (formerly called PCNM analysis, Section 14.1); generalized Moran's eigenvector maps (MEM, Section 14.2); asymmetric eigenvector maps (AEM) developed to model the effects of directional physical processes (Section 14.3); and multiscale ordination (Section 14.4). Section 14.5 describes derived methods of spatial analysis based on MEM, and

Section 14.6 is a rejoinder that shows how these methods can help answer questions involving the multiscale analysis of beta diversity. Section 14.7 lists R functions available to carry out the calculations.

## 14.1 Distance-based Moran's eigenvector maps (dbMEM)

The positions of study sites on a map are identified by their spatial coordinates. Subsection 13.2.1 has shown how geographic coordinates can be used in a form of geographic modelling known as spatial trend-surface analysis. In that method, the coordinates are used, either directly (i.e. without transformation) or in the form of a polynomial function, to model univariate or multivariate response data through multiple regression (Subsection 13.2.1) or canonical analysis (Section 13.5).

Another way to look at the relative positions of the study sites is to compute geographic distances among them and write these to a geographic distance matrix  $\mathbf{D}_{\text{Geo}}$ . A simple form of spatial eigenfunction analysis is obtained by modifying the geographic distance matrix  $\mathbf{D}_{\text{Geo}}$ , as explained below, and computing spatial eigenfunctions by eigen-decomposition. That form was described in three papers by Borcard & Legendre (2002), Borcard *et al.* (2004) and Legendre & Borcard (2006), where the spatial eigenfunctions were called *Principal Coordinates of Neighbour Matrices* (PCNM). They are a special class of a family of eigenfunctions called *Moran's eigenvector maps* (MEM) described in Section 14.2. The formerly called PCNM eigenfunctions are actually MEM eigenfunctions based on simple geographic distances; they are now called *distance-based MEM*, abbreviated dbMEM.

PCNM

MEM

dbMEM

The construction of dbMEM eigenfunctions is described in Subsection 14.1.1. After their construction, spatial eigenfunctions can be used in linear models of the response data in the same way as polynomials of geographic coordinates: they become explanatory variables in multiple linear regression when analysing univariate response data, e.g. species richness at different sites, or in canonical analysis when studying the spatial variation of multivariate response data, e.g. community composition. They can also be used as one of the explanatory matrices in variation partitioning aimed at analysing a matrix of response data from two or more angles. These aspects are illustrated through ecological applications presented in Subsection 14.1.3.

Ecologists who are not familiar with multiscale eigenfunction analysis may consider looking at the examples and ecological applications of Subsections 14.1.2 and 14.1.3 first, before coming back to study the algorithm in detail.

## 1 — Algorithm

The steps involved in the construction of dbMEM eigenfunctions are the following:

- Compute a matrix of geographic distances by applying the Euclidean distance function to a set of Cartesian geographic coordinates. Latitude-longitude data can be transformed into flat Cartesian coordinates using function *geoXY()* (Section 14.7). Alternatively, for sites covering a large geographic area on the Earth's surface, geodesic distances can be computed. The end product of this first step is a square symmetric matrix of distances among sites.
- Choose a distance threshold called '*thresh*' to truncate the geographic distances, separating them in two groups: small and large distances. This way of proceeding was inspired by the division of distances into distance classes in Mantel correlograms (Subsection 13.1.6). How to determine the value of the threshold is described below. The distances smaller than or equal to the threshold are kept as they are in the modified distance matrix  $\mathbf{D}_{\text{trunc}}$ . The distances larger than the threshold are replaced by an arbitrary large distance.  $\mathbf{D}_{\text{trunc}}$  is a truncated distance matrix because the distances larger than *thresh* have been removed and replaced by a large constant value. The value arbitrarily used in computer software is 4 times the value of the threshold. Any value larger than 4 would serve equally well the purpose of distorting the distance matrix and allowing spatial eigenfunctions to be computed from it, with little change to the numerical results.
- In dbMEM, the diagonal values of the distance matrix, which were originally zeros, are replaced by the value  $(4 \times \text{thresh})^*$ . This change on the diagonal of  $\mathbf{D}_{\text{trunc}}$  indicates that a site is not connected to itself; this is also the case in the computation of Moran's *I* coefficients in correlograms.
- Compute a principal coordinate analysis (PCoA, Section 9.3) of  $\mathbf{D}_{\text{trunc}}$  producing eigenvalues and eigenvectors. If PCoA were computed from  $\mathbf{D}_{\text{Geo}}$  instead, the relative positions of the sites would be recovered in a two-dimensional ordination of the points; so there would be two positive eigenvalues (or three for sites representing a large area on the Earth's surface), and all the other eigenvalues would be 0. Here, PCoA is applied to the distorted (truncated) matrix  $\mathbf{D}_{\text{trunc}}$ . The surprising consequence is the production of  $(n - 1)$  eigenvalues different from 0 and  $(n - 1)$  corresponding eigenvectors, instead of two. Some of the eigenvalues are positive, some are negative. The examples below will show the balance between positive and negative eigenvalues, and what they mean. In the calculation of eigenvectors, the signs along any one eigenvector can be switched among software or computer platforms, because the sign

---

\* In classical PCNM eigenfunctions, the diagonal values of  $\mathbf{D}_{\text{trunc}}$  are 0, indicating that a site is connected to itself. The eigenvalues of classical PCNM analysis are larger than those of dbMEM analysis by a constant equal to  $(4 \times \text{thresh})^2/2$ , so that there are artificially more positive eigenvalues in the PCNM than in the dbMEM solutions, but the eigenvectors, which are the spatial eigenfunctions, are identical to those computed by the dbMEM procedure described here.

of the first element of each eigenvector (+ or –) is assigned arbitrarily, as explained in Chapters 2 and 9.

- The principal coordinates, which are the spatial eigenfunctions, represent (or *model*) together the multiscale distance relationships among the sites. They can be used in the same ways as any other types of explanatory variables: they can be mapped (examples are shown below); or used as explanatory variables in linear modelling (multiple linear regression, generalized linear models, canonical analysis, etc.); or used in variation partitioning. Subsets of them can be selected by linear model selection procedures.

Moran's eigenvectors      The eigenfunctions computed in this way are called *Moran's eigenvectors* because their eigenvalues are equal to Moran's  $I$  coefficients of spatial correlation (eq. 13.1) computed for these eigenfunctions using the pairs of sites that remain connected after truncation, divided by a constant (Dray *et al.*, 2006). In the case of a linear transect with equispaced points (example developed below), about half the eigenvectors have positive Moran's  $I$  and model positive spatial correlation, and the other half have negative Moran's  $I$  and model negative spatial correlation at short range. In most ecological studies, only the eigenvectors with positive Moran's  $I$  are used to model the spatial correlation in data, but the eigenvectors with negative Moran's  $I$  are also available to model the response data. In studies of territorial animals, for example, the eigenfunctions with negative Moran's  $I$  allow researchers to test hypotheses formulated to explain the negative spatial correlation among the study sites.

How should the truncation threshold be chosen? The method for choosing the value of the threshold, *thresh*, derives from the observation that MEM eigenfunctions display variation across the full set of sites under study if the sites form a connected graph in matrix  $\mathbf{D}_{\text{trunc}}$ , meaning that there is chain of connections made of distances smaller than or equal to *thresh* linking all sites; the concept of  $G_c$ -chain is explained in Section 8.2. If there are, say, two groups of points (sites) with no connection between the groups, the variation within each group is modelled by subsets of dbMEM eigenfunctions that do not vary in the other group. This observation suggests the following method: to ensure that all points are modelled by the same set of eigenfunctions, choose the value of *thresh* in such a way that the distances smaller than or equal to *thresh* in  $\mathbf{D}_{\text{Geo}}$  form a  $G_c$ -chain linking all points in a connected graph. Disconnected pairs are identified in matrix  $\mathbf{D}_{\text{trunc}}$  by distances equal to  $(4 \times \text{thresh})$ . This leads to the following recommended method:

- Create a minimum spanning tree (MST, Sections 8.2 and 13.3.1) linking all points (sites) in the study. Identify the length of the largest edge in the chain forming the MST. An illustration is provided with Numerical example 3 below.
- Set *thresh* equal to the length of the largest edge in the MST, or any other value of the user's choice that is larger than that value. See the examples below. In practice, choosing a *thresh* value equal to the longest edge forming the MST maximizes the number of eigenfunctions that model positive spatial correlation. Although it is compatible with the definition of dbMEM eigenfunctions, choosing for *thresh* a value

larger than that reduces the number of eigenfunctions that model positive spatial correlation. The first few eigenvectors remain unchanged, but the following ones are changed. Hence it is recommended to routinely use the smallest possible truncation level for *thresh*, i.e. the value provided by the MST.

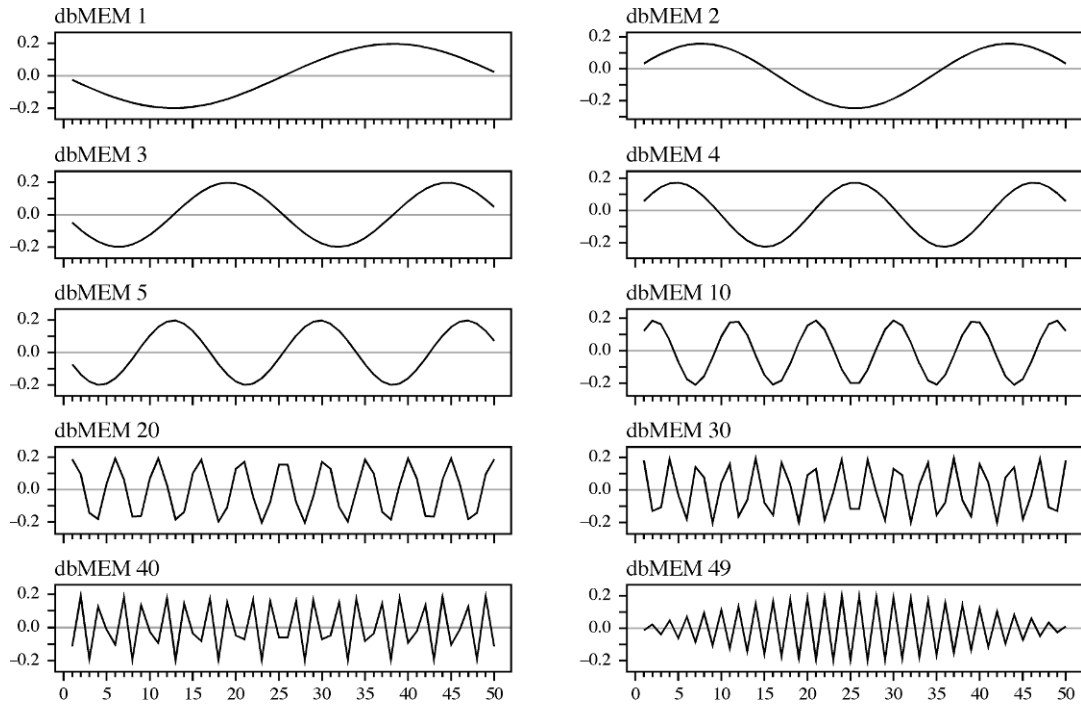
It may be interesting and appropriate in some studies to analyse together two or several disconnected groups of sites. In that case, separate sets of dbMEM eigenfunctions should be generated before analysing the spatial structure of response data observed at these sites, and assembled in a staggered matrix of eigenfunctions that will allow a single analysis to be conducted for the sites belonging to the separate groups. This is a far better practice than trying to create a single set of dbMEM eigenfunctions by choosing a large *thresh* value. Indeed, that would compromise the resolution of the analysis by affecting the fine-scale dbMEM eigenfunctions. Function ***create.MEM.model()*** described in Section 14.7 allows users to generate eigenfunctions for this type of analysis. An application is found in a study of the spatial metacommunity architecture of zooplankton in groups of pools located in separate valleys of the High Andes in Bolivia (Declerck *et al.*, 2011).

A MEM scalogram is a diagram representing the proportion of variance ( $R^2$ ) explained by the MEM eigenfunctions ordered along the abscissa by decreasing eigenvalues (Legendre & Borcard, 2006). For univariate response data  $\mathbf{y}$ , the scalogram can display the Pearson correlations, the regression coefficients, or the absolute values of the  $t$ -statistics associated with the regression coefficients computed between  $\mathbf{y}$  and the MEM eigenfunctions. Because the MEM eigenfunctions are orthogonal to one another, the partial regression coefficients obtained in a multiple regression of  $\mathbf{y}$  on all MEM eigenfunctions are equal to the simple regression coefficients between  $\mathbf{y}$  and each MEM eigenfunction in turn. For a multivariate response matrix  $\mathbf{Y}$ , the ordinate of the scalogram can display either the  $R^2$  explained by the various MEM eigenfunctions or the associated  $F$ -statistics. A  $t$ -value scalogram displays  $t$ -statistics obtained by multiple regression of a single response variable on the MEM eigenfunctions. An example of  $t$ -value scalogram is shown in Fig. 14.5 (Ecological application 14.1a).

## 2 — Numerical examples

This subsection examines numerical examples of dbMEM eigenfunctions produced for different sampling designs.

**Numerical example 1.** Consider a transect with 50 equally-spaced sites. Only the positions of the points along the transect are required for the generation of the inter-point distance matrix  $\mathbf{D}_{\text{Geo}}$  and the calculation of dbMEM eigenfunctions; the point positions were represented by the integers 1 to 50 for the calculations, but they could have been given by any other series of 50 equally-spaced values. There were 49 non-zero eigenvalues and 49 corresponding eigenvectors produced. The eigenvalues, ranging from the largest ( $\lambda_1 = 14.9$ ) to the smallest ( $\lambda_{49} = -15.0$ ), ordered the eigenfunctions by wavelengths, from broad scale to fine scale. Twenty-four eigenvectors had positive eigenvalues and Moran's  $I$ , and 25 eigenvectors had negative eigenvalues and Moran's  $I$ .



**Figure 14.1** Graphs of ten of the 49 dbMEM eigenfunctions that represent the spatial variation along a transect with 50 equally-spaced points. Abscissa, from left to right: sites 1 to 50. Ordinates: values along the dbMEM eigenfunctions.

Figure 14.1 shows some of the 49 eigenfunctions that were produced. The first seven eigenfunctions illustrated in the figure (dbMEM 1 to 5, 10, 20) belong to the group modelling positive spatial correlation. dbMEM 30, 40 and 49 displays negative spatial correlation at small distances; indeed, these eigenfunctions have negative Moran's  $I$  values. The values along each eigenfunction form a sine wave. Signs may be reverted along any one eigenfunction because different software, or the same software running on different computer platforms, can produce switched signs along any of the eigenvectors in PCoA. The wavelengths of eigenfunctions are rarely integer multiples of the sampling interval. Because the eigenfunctions are only computed and plotted at the 50 sampling points, interference generates amplitude-modulation (AM) waves in panels dbMEM 30, 40 and 49, although the eigenfunctions are perfectly correlated with sine waves.

Guénard *et al.* (2010, eq. 3) showed that for a transect containing  $n$  regularly-spaced points and with sampling interval  $s$ , the wavelength  $\lambda_i$  of the sine wave corresponding to the eigenfunction with rank  $i$  is:

$$\lambda_i = 2 \frac{(n + s)}{(i + 1)} \quad (14.1)$$

For example, for a 50-point transect as the one used to compute Fig. 14.1, the complete sine wave of dbMEM 1 has a wavelength of 51 units (eq. 14.1), compared to the length of the transect which is  $50 - 1 = 49$  inter-point units, assuming sampling points with negligible size. The following eigenfunctions form sine waves of shorter wavelengths, as predicted by eq. 14.1. The last eigenfunction shown in Fig. 14.1, dbMEM 49, has a wavelength of 2.04; hence it is not in phase with the set of points that are spaced by 1 unit and a false wave that has the length of the series modulates the amplitude of the sine wave in the envelope of the eigenfunction graph (amplitude modulation, or AM, wave). When the points are irregularly-spaced along a transect, the sine waves are deformed, but one can still recognize the eigenfunctions that model broader-scaled and finer-scaled phenomena. Examples are given by Borcard *et al.* (2004, Appendix C).

**Numerical example 2.** Surveys of permanent forest plots\*, as well as many field experiments, are conducted on regular grids of points. A regular  $12 \times 8$  grid (96 points) was generated for the present example to illustrate dbMEM eigenfunctions on regular grids. The eigenfunctions were computed for that grid using a *thresh* value of 1, which corresponded to the distance between adjacent points in the horizontal and vertical directions. There were a total of 95 eigenvalues and corresponding eigenfunctions. The first 48 eigenfunctions modelled positive spatial correlation† and the last 47 modelled negative spatial correlation.

Figure 14.2 shows maps of ten of the 48 eigenfunctions modelling positive spatial correlation. The patterns alternate between vertical, horizontal, and diagonal contrasts. The two central horizontal lines of points in the map of dbMEM 1 have the same large sine wave shape as dbMEM 1 in Fig. 14.1: the values go from 0 (grey) on the left, to negative values (white), to 0 (grey) in the centre of the lines, to positive (black), and back to 0 (grey) on the right.

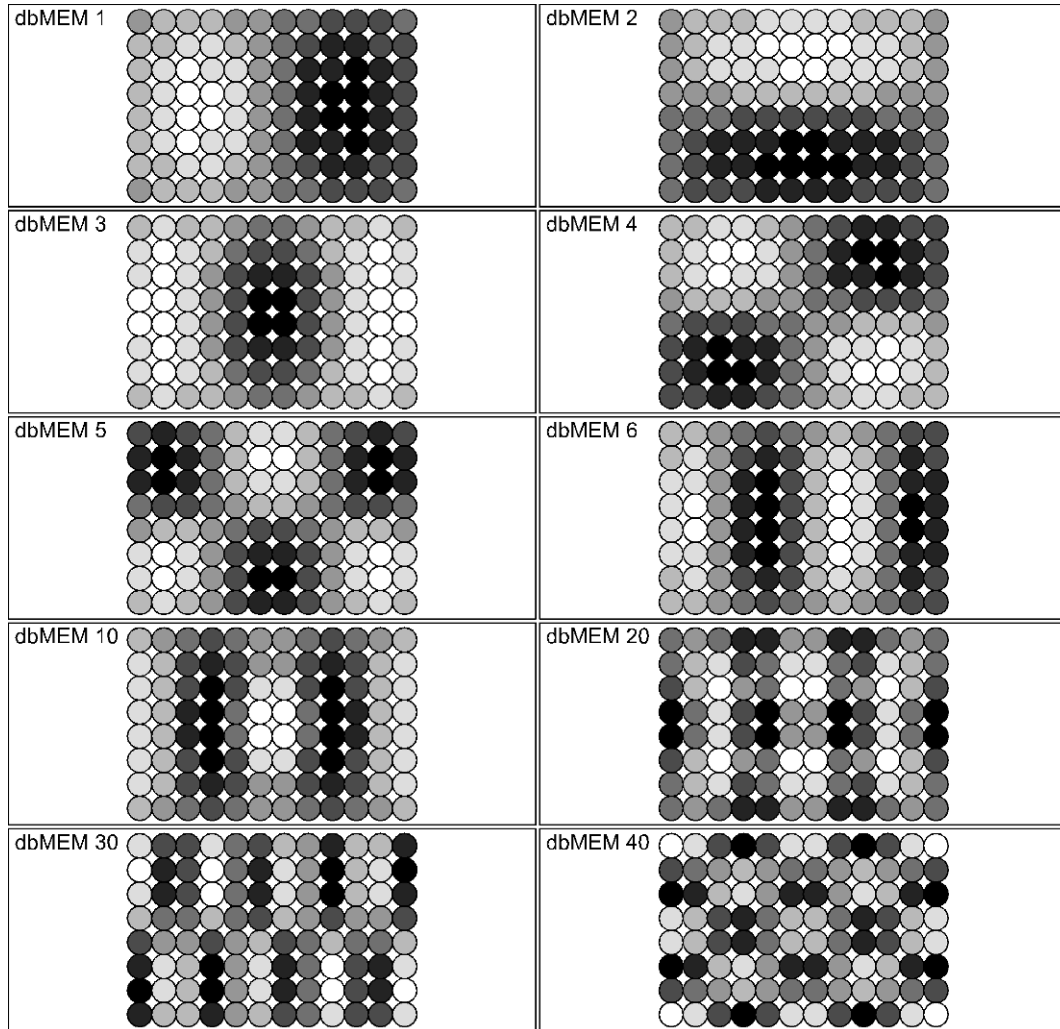
For a square regular grid of points, many of the pairs of successive eigenfunctions produced during dbMEM generation have multiple eigenvalues (Section 2.10, third property), creating situations of circularity. Different software, or different computer platforms using the same software, may produce pairs of eigenvectors that are rotated differently. Note, however, that these pairs of eigenfunctions explain together the same amount of variation in the data, whatever the rotation. In any case, the patterns on some eigenfunction maps are symmetric while for pairs of multiple eigenvalues, successive maps display the same pattern with a  $90^\circ$  rotation. Borcard *et al.* (2011, Fig. 7.4) showed spatial eigenfunction maps for a square grid of points.

**Numerical example 3.** Nine points were used to illustrate the construction of connection networks in Figs. 13.22 to 13.24. These points are used again here to compute dbMEM

\* See note on the CTFS permanent forest plots in Subsection 6.5.3 and Ecological application 14.1b where one of those forest plots is analysed.

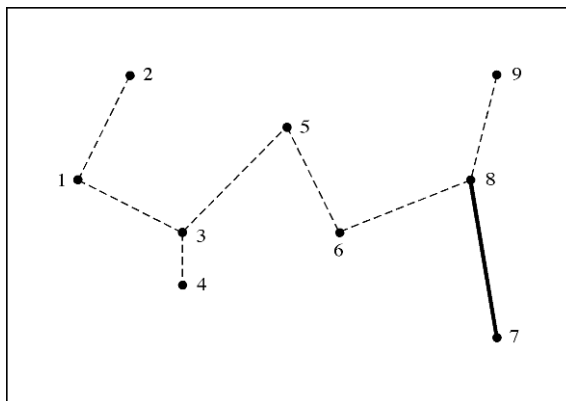
† The expected value of Moran's  $I$  under the null hypothesis regarding the absence of spatial correlation is a small negative value,  $E(I) = -(n-1)^{-1}$  (eq. 13.6). Sometimes, as in the present example, it happens that a dbMEM eigenfunction has a small negative Moran's  $I$  value that is larger than  $E(I)$ , and thus also has a small negative eigenvalue. In the example, eigenfunction 48 had a Moran's  $I$  value of  $-0.00948$ , which is larger than  $E(I) = -0.01053$ ; it was counted among those that modelled positive spatial correlation.





**Figure 14.2** Bubble maps showing ten of the 48 dbMEM eigenfunctions that display positive spatial correlation. Shades of grey represent the values in each eigenvector, from white (largest negative value) to black (largest positive value). Signs may be reverted in the construction of the eigenvectors with no consequence for the analysis; reverted signs would interchange black and white in the panels. The maps were produced using function *sr.value()* (Section 13.6).

eigenfunctions. Figure 14.3 shows the minimum spanning tree computed from the spatial coordinates of the points found in Fig. 13.22. The longest edge along the tree has a length of 3.04 units; that length was used as the *thresh* value for the computation of the truncated distance matrix  $\mathbf{D}_{\text{trunc}}$ . Figure 14.4 shows maps of the eight eigenfunctions produced by dbMEM

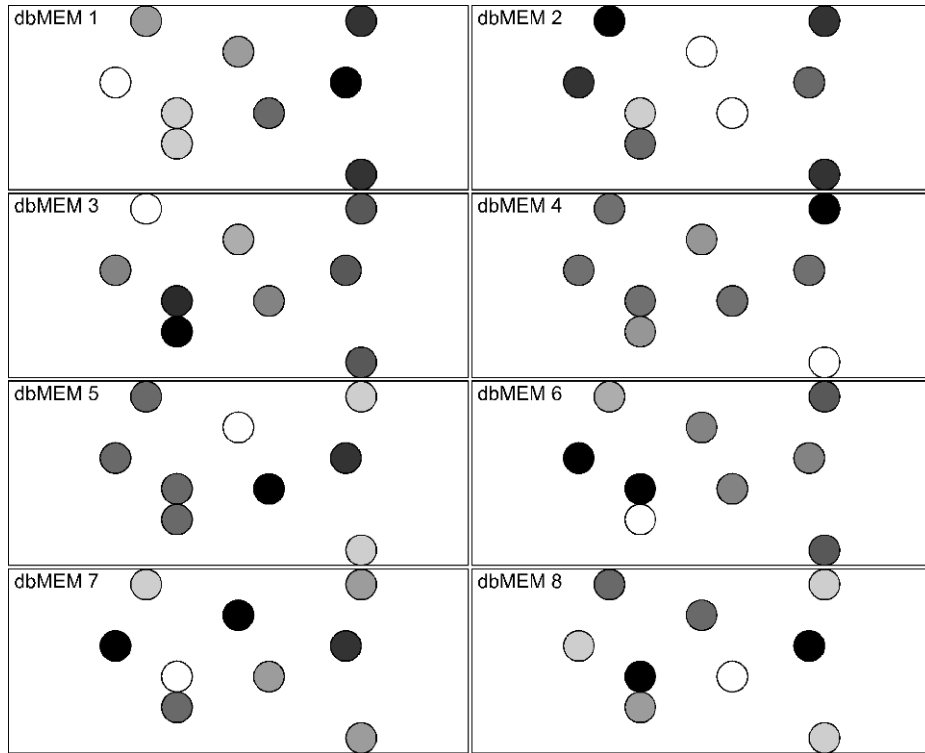


**Figure 14.3** Minimum spanning tree of the nine points from Fig. 13.22. The longest edge, between points 7 and 8, is in bold; its length (3.04) is used as the *thresh* value. The dashed edges are shorter.

decomposition: four display positive spatial correlation and have positive eigenvalues and Moran's  $I$ , and four display negative spatial correlation and have negative eigenvalues and Moran's  $I$ . The map of dbMEM 1, for example, displays a gradient between negative values (white) on the left and positive values (black) on the right. dbMEM 2 contrasts the centre of the map (white circles) with the left and right edges (dark grey and black circles). The last maps have circles with contrasting shades side by side, picturing negative spatial correlation at short range.

An important methodological point concerns the analysis of data that embed a linear spatial gradient. A linear gradient can be modelled by dbMEM eigenfunctions. Along a regular transect, for example, the even-numbered dbMEM eigenfunctions can be used together in a linear function to model a linear gradient almost perfectly, i.e. with a very high  $R^2$ . This is because the even-numbered eigenfunctions (1, 3, 5, etc.) are asymmetrically positioned with respect to the centre of the transect, as can be seen in Fig. 14.1. The odd-numbered eigenfunctions (2, 4, 6, etc.), on the contrary, have symmetrical shapes with respect to the centre of the transect and cannot be used to model a linear gradient. This being said, it is not good practice to use eigenfunctions to model a gradient. There are two reasons for this. Firstly, a gradient can be seen as a portion of a spatial structure that is much larger than the study area. Nothing will be learned by using half of the eigenfunctions to model such a structure, which can be modelled more simply by a linear function of the positions of the sites along a transect or their geographic coordinates on a surface. Secondly, if eigenfunctions are used to model a linear gradient, they cannot be used to model more interesting spatial structures. As a consequence, when the response data contain a linear gradient in one or two geographic dimensions, it is recommended to detrend them prior to MEM analysis (Subsection 13.2.1).

Detrend  
the data



**Figure 14.4** Bubble maps showing the eight dbMEM eigenfunctions for the nine points from Fig. 13.22. The first four model positive spatial correlation. Shades of grey: see Fig. 14.2.

Users of spatial eigenfunction analysis are warned against the temptation to interpret a single MEM eigenfunction that happens to fit well a spatial structure that can be observed in response data. Had the set of study points be offset with respect to the actual study area, for instance to the east or to the west, that MEM would probably not fit the response data so well, or not at all, and the structure would then be fitted by other eigenfunctions. The message here is that users should look for sets of MEM eigenfunctions, corresponding to a given spatial scale, that, together, fit response data fairly well, not individual eigenfunctions.

### 3 — *Ecological applications*

Many applications of spatial eigenfunction analysis of the dbMEM type are available in the ecological literature. Three of those are summarized here.

### Ecological application 14.1a

This application illustrates dbMEM analysis for a single response variable along a transect of equally-spaced sampling sites. Borcard *et al.* (2004) reanalysed data originally collected and analysed by Tuomisto & Poulsen (2000) who surveyed the fern assemblages (32 species) along a 1300 m transect in the tropical forest, in the Huanta region of the Upper Amazonian River in northeastern Peru. The response variable examined in the present application is the abundance of the fern *Adiantum tomentosum* Klotzsch in 260 adjacent  $5 \times 5$  m quadrats. Explanatory environmental variables were also collected along the transect. The objective of the study presented by Borcard *et al.* (2004) was to determine the spatial scales at which the abundance of the species was structured, and relate these scales to environmental variables that were hypothesized to affect the spatial distribution of the species.

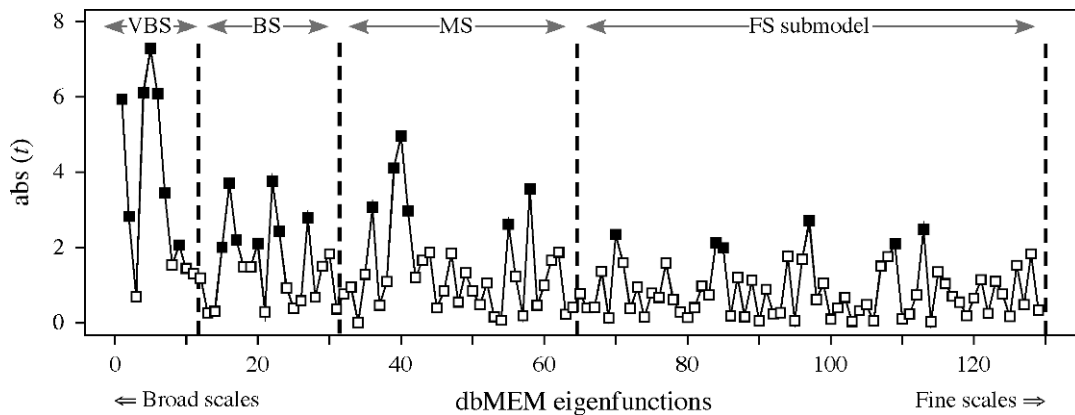
In the analysis of the Huanta fern data, Borcard *et al.* (2004) used all 176 PCNM eigenfunctions that had positive eigenvalues. These corresponded to dbMEM eigenfunctions 1 to 129 that modelled positive spatial correlation plus the first 47 dbMEM that modelled negative spatial correlation. In the analysis recomputed for the present application, only the 129 dbMEM that modelled positive spatial correlation were used; this corresponds to present-day practice. The changes to the results are small as can be seen by comparing the present results to those shown in Appendix B of Borcard *et al.* (2004). A dbMEM model could also be developed based on the eigenfunctions that model negative spatial correlation; such a model, if significant, would display avoidance phenomena.

Prior to analysis against the dbMEM and environmental variables, the abundance data were square-root transformed to make the distribution of abundances more symmetrical, albeit not strictly normal. There was no significant spatial trend in the data, so no detrending was carried out. The dbMEM eigenfunctions were computed along the transect; the integers 1 to 260 represented quadrat positions along the transect. Among the 129 dbMEM that had positive Moran's  $I$  values and thus modelled positive spatial correlation, 26 significant eigenfunctions ( $p \leq 0.05$ ) were identified by forward selection (Section 11.1.10, paragraph 7). In the scalogram (Fig. 14.5), these eigenfunctions are identified by black symbols. These same 26 eigenfunctions were also significant in a multiple regression of the response variable against the 129 dbMEM eigenfunctions.

Together, these 26 significant eigenfunctions formed a descriptive model with  $R_a^2 = 0.568$ . They were divided into four submodels as shown in the scalogram (Fig. 14.5): the first seven dbMEM were called the very-broad-scale (VBS) submodel, the next seven the broad-scale (BS) submodel, the next six the medium-scale (MS) submodel, and the last six formed the fine-scale (FS) submodel. Natural clusters of significant values can be seen in the scalogram, especially for the first two groups; they helped divide the dbMEM into submodels. Because there is a single response variable in this application, i.e. the *Adiantum tomentosum* fern abundance, fitted values were computed by regression of the species data on the eigenfunctions forming each submodel. These fitted values are shown in Fig. 14.6 b-e. All submodels were statistically significant.

The next step of the analysis was to identify the environmental variables that corresponded to the different submodels.

- The very-broad-scale (VBS) submodel was explained by six variables that were significant in forward selection ( $R_a^2 = 0.382$  with respect to the variance in the VBS fitted values): quadrat elevation (this variable was detrended against quadrat positions along the transect prior to the analysis), trees 3-7.5 cm dbh (dbh is diameter at breast height), trees 31.5-62.5 cm dbh, lianas 8-15 cm diameter, thickness of soil organic horizon, canopy height.

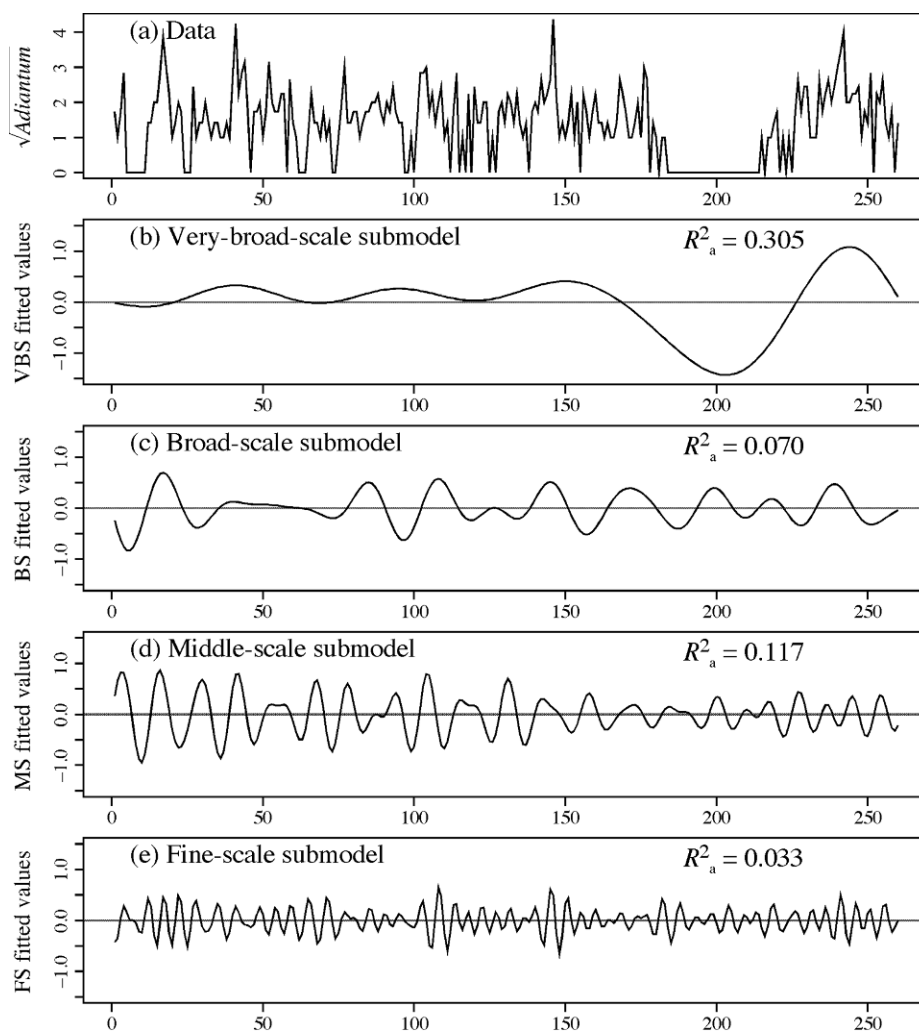


**Figure 14.5** Scalogram of the fern *Adiantum tomentosum* multiscale structure along the Huanta transect. Abscissa: the 129 dbMEM eigenfunctions with positive Moran's  $I$ . Ordinate: absolute values of the  $t$ -statistics. The 26 eigenfunctions selected by forward selection ( $p \leq 0.05$ ) are identified by black squares. Dashed lines indicate the divisions into the VBS, BS, MS and FS submodels.

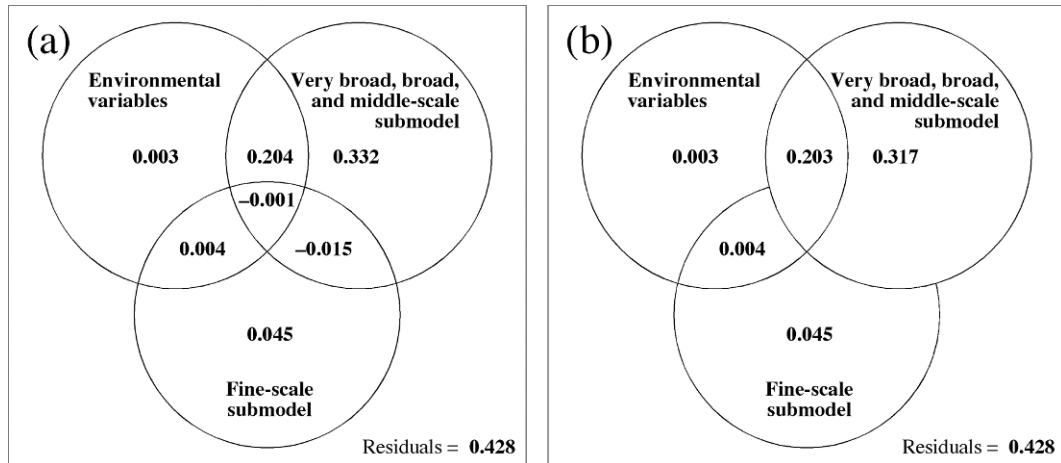
- The broad-scale (BS) submodel was explained by a different linear model containing two of the same variables as in the VBS submodel ( $R_a^2 = 0.124$  with respect to the variance in the BS fitted values): quadrat elevation, and lianas 8–15 cm diameter.
- The medium-scale (MS) submodel was explained by two variables ( $R_a^2 = 0.064$  with respect to the variance in the MS fitted values): waterlogging (saturation of the soil by groundwater), which was not selected in the VBS and BS submodels, and canopy height.
- The fine-scale (FS) submodel was not explained by any of the environmental variables that were available for the analysis.

In multiscale analysis of ecological data, one often finds that the fine-scale submodel is not explained by the available environmental variables, although the eigenfunctions composing it are significant. One remains uncertain as to the interpretation to give to this observation: either the environmental variables that could explain the fine-scale variation have not been measured, or the fine-scale spatial structure displayed by the response data is not due to environmental control (Chapter 1, eq. 1.1) but represents autocorrelation (eq. 1.2) generated by the dynamics of the population (in the present example), or by community dynamics when studying community composition data. This question of interpretation is revisited in Subsection 14.1.4.

Variation partitioning (Subsections 10.3.5 and 11.1.11) was performed with respect to (1) the seven environmental variables selected above, (2) the 20 dbMEM eigenfunctions forming submodels VBS, BS and MS that are related to the environmental variables, and (3) the six dbMEM eigenfunctions forming the FS submodel. Figure 14.7a shows the partitioning results. Even though the two sets of dbMEM eigenfunctions were uncorrelated, subtraction of  $R_a^2$  coefficients artificially created small negative values in the fractions of the partition corresponding to intersections between the dbMEM submodels; these small values should be interpreted as zeros. This annoying problem can be corrected by creating a hierarchy among the



**Figure 14.6** MEM analysis of the fern *Adiantum tomentosum* in the Huanta transect, Peru. Abscissa: quadrat positions along the transect. (a) Square-root transformed abundances. Zero values were observed in portions of the transect. (b) Fitted values of very-broad-scale (VBS) submodel, centred (seven dbMEM); (c) of broad-scale (BS) submodel (seven dbMEM); (d) of medium-scale (MS) submodel, (six dbMEM); (e) of fine-scale (FS) submodel (six dbMEM). The adjusted  $R^2$  of each submodel is shown. The ordinate scale is the same in graphs b-e to emphasize differences in explained variation among submodels.



**Figure 14.7** (a) Venn diagram presenting the variation partitioning results for the fern *Adiantum tomentosum* along the Huanta transect. The fraction values displayed are computed from adjusted  $R$ -squares ( $R_a^2$ ). (b) Same partition with hierarchical partitioning, which keeps the two sets of dbMEM orthogonal (intersection fractions = 0). The diagram on the left is the one produced by function *varpart()* of the VEGAN package in R, onto which text was added.

eigenfunction submodels in the analysis, or by apportioning the  $R_a^2$  of the intersection fractions proportionally to the variation explained by each submodel (Legendre *et al.*, 2012). In the present application, if one applies hierarchical partitioning and states that the (VBS, BS and MS) submodel has priority over the FS submodel, then the (VBS, BS and MS) submodel is served first in the variance resource and secures for itself the small negative fractions found in the intersection with the FS submodel. As a result, the intersection in explained variation between the two submodels has disappeared in Fig. 14.7b.

Nearly all the among-site fern variation explained by the environmental variables was also explained by the eigenfunctions, showing that it was spatially structured. The first three spatial submodels, grouped in the upper-right circle of Fig. 14.7b, accounted for about half (52%) of the among-site variation of fern abundances, and  $(0.203/0.520) \approx 40\%$  of that explained variation was shared with the environmental variables, pointing to an environmental control of that portion of variation. This left about 60% of that variation unexplained by the environmental variables. The fine-scale submodel explained much less of the fern abundance variation, but very little of that variation was shared with the environmental variables, suggesting that a different process was at work that generated this smaller amount of explained variation.

#### Ecological application 14.1b

This application illustrates dbMEM analysis for a multivariate response matrix on a regular grid positioned on a geographic surface (map). Data from a 24-ha permanent forest plot established and surveyed in 2005 in the Gutianshan National Nature Reserve in the Zhejiang Province of

China were analysed by Legendre *et al.* (2009) to determine how much of the spatial variation in species composition (beta diversity) was spatially structured, and of that, how much variation was related to the topography of the forest plot. The forest plot was fully surveyed, i.e. all 140676 trees with diameter at breast height (dbh) larger than 1 cm were tagged, identified to species, measured, and georeferenced. The trees belonged to 49 families and 159 species. The climate of the plot (29°15'N) is subtropical. The Gutianshan plots is a member of the CTFS network (see footnote in Subsection 6.5.3).

For the analysis, the forest plot was divided in the computer into cells of 20 × 20 m. The first part of the spatial analysis was based on those 600 cells. There were between 19 and 54 tree species per cell. Four topographic variables were available. Three of them (altitude, convexity of the cells, and slope) were developed into cubic polynomials to allow these variables to model nonlinear relationships with the tree species abundances, thus increasing their explanatory power; see polynomial regression, Subsection 10.3.4. The fourth variable, aspect, is a circular variable; it was transformed into two new variables, sin(aspect) and cos(aspect), which allowed their use in linear models.

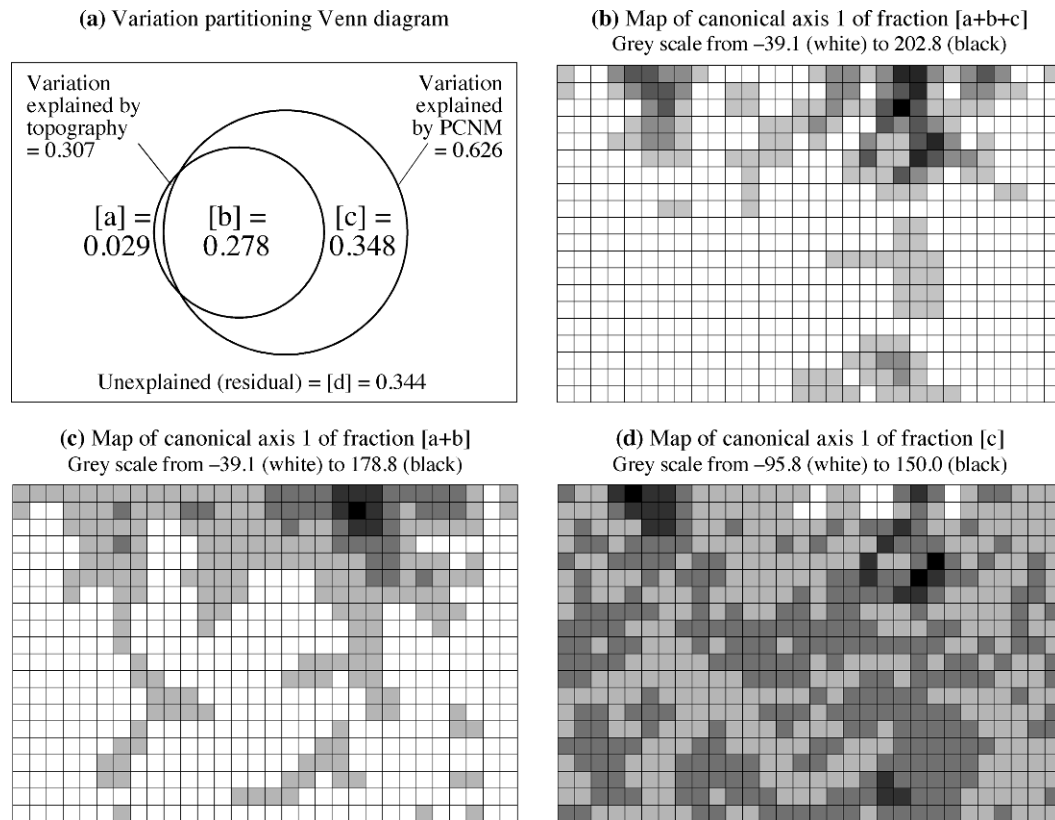
339 PCNM eigenfunctions (now called dbMEM) were used in the analysis without any selection. Indeed, the  $R_a^2$  statistic obtained from the analysis of the community composition data by the full set of 339 PCNM ( $R_a^2 = 0.626$ ) was nearly identical to that obtained after forward selection of 179 eigenfunctions that were significant at the 0.05 level ( $R_a^2 = 0.625$ ). The 339 PCNMs included 200 functions with positive Moran's  $I$ , which modelled positive spatial correlation, and 139 with negative Moran's  $I^*$ . Among the first 180 eigenfunctions, nearly all significantly explained the tree community variation; these eigenfunctions represent broad to medium-scale variation.

The variation partitioning results (Fig. 14.8a) indicated that 63% of the among-cell variation ( $R_a^2$ ) of the community composition (159 species) was spatially structured and explained by the 339 spatial eigenfunctions. Nearly half of that ( $0.278/0.626 = 44\%$ ) was also explained by the four topographic variables. Without surprise, nearly all the variation explained by the topographic variables was shared with the spatial eigenfunctions. The spatially-structured fraction of variation unexplained by the topographic variables ( $R_a^2 = 0.348$ ) could be related to unmeasured environmental variables, like soil chemistry, or it may have been generated by community dynamics, including neutral processes (Subsection 1.1.1).

For multivariate response data, variation partitioning is computed using RDA (Section 11.1) instead of multiple regression. The total variation of the community composition data by the table of topographic variables (fraction [a+b] of the Venn diagram in Fig. 10.10), and that of the joined tables of topographic and PCNM variables (fraction [a+b+c]), were partitioned into a number of orthogonal canonical axes by RDA. The table of fitted values corresponding to [c], the fraction uniquely explained by the PCNM variables, was computed by partial RDA, which also partitioned it into orthogonal canonical axes. Maps of the first canonical axis of each of these analyses are presented in Fig. 14.8b-d. Note that these maps are not additive, i.e. the values on the map of [a+b+c] are not equal to the values on the map of [a+b] plus those on the map of [c], because the production of orthogonal axes is done separately by the three canonical analyses. The interpretation of these maps is not as straightforward as for univariate response

\* In classical PCNMs, some of the eigenfunctions with negative Moran's  $I$  have positive eigenvalues, as explained in the footnote of Subsection 14.1.1. These eigenfunctions were not used when the analysis was repeated with only the 200 dbMEM eigenfunctions with positive Moran's  $I$ . That analysis produced nearly identical variation partitioning results as in Fig. 14.8a.



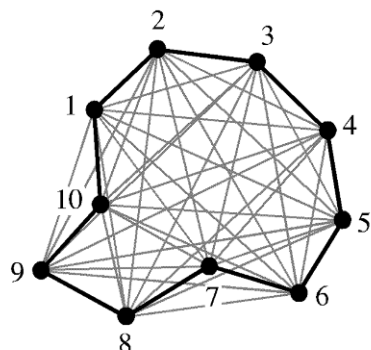


**Figure 14.8** (a) Venn diagram: variation partitioning of the Gutianshan forest community composition with respect to topographic variables and spatial eigenfunctions. (b-d) The Gutianshan forest plot was divided into 600 cells of  $20 \times 20$  m. Maps of canonical axis 1 of (b) fraction [a+b+c] (43% of the species variation, unadjusted  $R^2$ ), (c) fraction [a+b] (24% of the species variation), (d) fraction [c] (14% of the species variation). Values in the cells are represented by shades of grey as shown above each map. Modified from Legendre *et al.* (2009).

data. These maps are useful, though, because they allow ecologists to visualize the spatial variation on separate canonical axes for each fraction of variation separately.

In addition to the  $20 \times 20$  m cells, the forest plot was also divided in the computer into cells of sizes  $10 \times 10$  m,  $40 \times 40$  m, and  $50 \times 50$  m. These four cell sizes allowed divisions of the 24-ha plot into cells of equal sizes that added up to the whole plot. The variation of the four resulting community tables was partitioned as described for the  $20 \times 20$  m cell data. Comparison of the results showed that the effect of the topographic variables (fraction [a+b]) increased with cell size whereas the variation uniquely modelled by the eigenfunctions ('pure' spatial variation, fraction [c]) decreased. Hence the perceived balance between environmental and spatial effects varies with the size of the sampling units ('grain size' in Section 13.0).

(a) Sites along the shoreline

(b)  $\mathbf{D}_{\text{trunc}}$  matrix

Sites	1	2	3	4	5	6	7	8	9	10
1	—									
2	1	—								
3	4	1	—							
4	4	4	1	—						
5	4	4	4	1	—					
6	4	4	4	4	1	—				
7	4	4	4	4	4	1	—			
8	4	4	4	4	4	4	1	—		
9	4	4	4	4	4	4	4	1	—	
10	1	4	4	4	4	4	4	4	1	—

**Figure 14.9** Example of construction of dbMEM eigenfunctions for a loop sampling design. (a) Ten sites located along the shoreline of a lake. The lines representing the distances between neighbouring sites along the shore are in bold. (b) Truncated distance matrix  $\mathbf{D}_{\text{trunc}}$ : the neighbouring sites are at distance of 1 in this sketchy example; non-neighbouring sites (grey lines in panel a) receive values  $4 \times \text{thresh}$ , where  $\text{thresh} = 1$ . Diagonal values (=4) not shown. Redrawn from Brind'Amour *et al.* (2005).

### Ecological application 14.1c

This application illustrates dbMEM analysis of multivariate response data in a non-standard sampling situation. Freshwater fish were censused by snorkelling at 90 sites in the littoral zone of a small lake; the data were analysed by Brind'Amour *et al.* (2005). The littoral zone of a lake forms a loop instead of a transect. The same situation occurs when sampling the beach around an island or the ecotone\* around a forest patch. To compute dbMEM eigenfunctions in such a situation, one must proceed as follows (Fig. 14.9):

- Calculate the distances between adjacent sites along the sampling loop (e.g. the shoreline in the Brind'Amour *et al.*, 2005, fish data). The largest of these distances provides the *thresh* value.
- Construct matrix  $\mathbf{D}_{\text{trunc}}$ : keep the original distances between the neighbouring sites as they are in the distance matrix. Recode the distances between non-neighbouring sites to  $4 \times \text{thresh}$ . The value of *thresh* is 1 in the simplified example of Fig. 14.9; in a real study, it would be the largest distance between adjacent sites. Values 1 are found in the subdiagonal row of matrix  $\mathbf{D}_{\text{trunc}}$ . An additional value 1 between sites 10 and 1 closes the loop. The diagonal of  $\mathbf{D}_{\text{trunc}}$  receives values of  $4 \times \text{thresh}$  to produce dbMEM eigenfunctions (Subsection 14.1.1).

\* An ecotone is a transition area between two adjacent and different patches of landscape, such as forest and grassland.

For the 7-species fish community found in the small study lake, Brind'Amour *et al.* (2005) used RDA (Section 11.1) to compute dbMEM models corresponding to four scales: very broad, broad, middle, and fine scale. The community data were Hellinger-transformed (Section 7.7) prior to RDA. For interpretation, the first canonical axis of matrix **Z** (eq. 11.18) corresponding to each submodel was related by multiple regression to an explanatory matrix of environmental variables.

Besides the *Adiantum tomentosum* variable studied in Ecological application 14.1a, three other ecological data sets were analysed by Borcard *et al.* (2004): marine zooplankton collected along transects in Guadeloupe, chlorophyll *a* in a brackish lagoon in southern France, and the oribatid mite data also used in Ecological application 11.5. Other examples are: Jones *et al.* (2008: fern community composition across 1045 circular plots in an old growth rain forest in Costa Rica); Léonard *et al.* (2008: macrophyte community composition in 232 quadrats sampled along 24 transects in a fluvio-lacustrine underwater landscape); Arias-González *et al.* (2008: fish and coral community composition among reefs, and among reef types within reefs, in the western Caribbean Sea); Declerck *et al.* (2011: application briefly described at the end of Subsection 14.1.1); Bellchambers *et al.* (2011: distribution of spider conch in the Cocos Islands); Astorga *et al.* (2011: spatial variation of macroinvertebrate species richness in headwater streams at two spatial scales in Finland); Andersen *et al.* (2011: environmental control and spatial structures in peatland vegetation); Legendre & Birks (2012: analysis of fossil diatom assemblages (139 taxa) in a sediment core from south-western Scotland covering the past 10000 years).

Applications are also found in the field of hydrology. — Lacey *et al.* (2007) and Roy *et al.* (2010): modelling turbulent flow in a river in Québec; Noorduijn *et al.* (2010): water table response to alley farming of trees in Western Australia; Ali *et al.* (2010): soil moisture patterns in relation to hydrometeorological variables and topography in a forested catchment in Québec.

#### 4 — Interpretation of the fractions

In simple regression or canonical analysis modelling, one is interested in interpreting the variation of the response data (vector **y** or matrix **Y**) that is accounted for by the explanatory variables (matrix **X**) according to a model of causal relationships stated prior to the analysis. That model may be formulated loosely or stated quite precisely. The fraction of variation explained by the model is estimated by the adjusted coefficient of determination ( $R_a^2$ ) in multiple regression (eq. 10.21) and in RDA (eq. 11.5). The residual variance is assumed to be a random error component.

There may be two reasons for decomposing the variation of response vector **y** or matrix **Y** into additive components through the variation partitioning approach (Subsections 10.3.5 and 11.1.11). Fractions [a], [b] and [c] referred to in the following paragraphs are shown in Fig. 10.10.

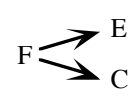
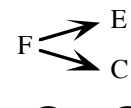

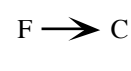

- If the spatial structure is considered to be a source of false correlations, i.e. that are not indicative of causal relationships, fraction [b] measures the interference of the spatial variables with the analysis of the relationship between **Y** and **X**. Fractions [b] and [c] should not be interpreted separately in that case, although one may still be interested in modelling the spatial structure of **Y** (fraction [b + c]) in a different analysis. As explained in Subsection 14.5.3, corrected tests of significance of fraction [a], which measures the effect of the **X** variables on **Y**, are obtained by incorporating MEM eigenfunctions as covariables in partial RDA to control for spatial correlation.
- If both the spatial and non-spatial structures of the explanatory variables are considered causal to the spatial variation of **Y**, fraction [a + b] estimates the amount of variation of **Y** explained by **X**. In such a case, the residuals of the analysis of **Y** by **X** are assumed to contain two identifiable fractions: [c], which is spatially structured, and [d], which is the random error component. A test of significance allows one to determine, at some confidence level  $\alpha$ , if [c] accounts for a significant fraction of the variation of **Y**. When that is the case, one should try to interpret fraction [c]. The next step is to “explain away” fraction [c] if possible. In other words, one should try to make fraction [c] fade away by adding explanatory variables (if available) to matrix **X** and recomputing the model. Mapping the site scores for the significant canonical axes of fraction [c] may help identify the processes responsible for this fraction of variation (Borcard & Legendre, 1994). Section 1.1 has shown, however, that spatial structures found in communities may originate from neutral processes of population and community dynamics (eq. 1.2) in addition to spatial dependence on environmental factors (eq. 1.1), so that not all the spatial variation in **Y** may be explainable by **X**.

In statistical analysis, causality, if invoked, resides in the hypotheses of the researcher (Subsection 4.5.4). The objective of causal statistical modelling is to assess how much of the observed variation can be explained by a consistent body of hypotheses (i.e. a set of compatible hypotheses). Problems of interpretation may occur, however, when important causal factors are left out of the model. The amount of variation of **Y** explained by the model may be small and, if these factors are causally anterior to both the variables in **Y** and some of the variables in set **X**, false correlations may appear in the model; this is also the case in path analysis (Section 10.4).

In community analysis, researchers are faced with a multiplicity of potential causal agents acting at a variety of spatial and temporal scales, thus creating a network of interactions that may be difficult to untangle. Section 13.0 mentioned three general models often invoked to explain community variation: the environmental control model (ECM), the biotic control model (BCM), and historical dynamics (HD). The latter refers to past natural events, such as isolation by geographic barriers and disturbances of various kinds (e.g. storms, forest fires, volcanic eruptions, landslides), and to anthropogenic causes such as agriculture, logging, mining, and constructions of various sizes (Plate 14.1, p. 906). These factors are usually not explicitly represented by variables in **X**. Some of these events may be traced by researchers (e.g. tornadoes, forest fires, logging, past agricultural plots) and explicitly included in a second round of modelling, while others cannot and may only be invoked in general terms to account

**Table 14.1**

Causal factors invoked to explain the fractions of variation [a] to [d] of Fig. 10.10, assuming that matrix **W** contains spatial eigenfunctions. The table focuses on the correlations between environmental variables (matrix **X**) and community composition (matrix **Y**). The following hypotheses are invoked: environmental control model (ECM), biotic control model (BCM), historical dynamics (HD), and spatial autocorrelation. Bullets: factors explicitly stated in the model; asterisks: factors not explicitly spelled out. Arrows: causal relationships. Modified from Borcard & Legendre (1994).

Fraction	Causal factors	Process	Causal model <sup>1</sup>
[a]	• Non-spatially-structured component of environmental or biotic factors	ECM BCM	$E \rightarrow C$
	* Non-spatially-structured environmental or biotic factors not included in the analysis	ECM BCM	
	* Historical events without spatial structure at the scale of the study	HD	
[b]	• Spatially-structured component of biotic or environmental factors included in the analysis	ECM BCM	$E \rightarrow C$
	* Spatially-structured environmental or biotic factors not included in the analysis	ECM BCM	
	* Spatially-structured historical events	HD	
	* Spatial autocorrelation in <b>X</b> and <b>Y</b>	Spatial autocorrelation	
[c]	* Spatially-structured environmental or biotic factors not included in the analysis	ECM BCM	
	* Spatially-structured historical events	HD	
	* Spatial autocorrelation in matrix <b>Y</b>	Spatial autocorrelation	
[d]	* Environmental or biotic factors not included in analysis and not spatially structured at scale of study	ECM BCM	
	* Historical events not included in analysis and not spatially structured at scale of study	HD	
	• Random variation, sampling error, etc.	Noise	

<sup>1</sup> C: community structure (matrix **Y**)

E: factor explicitly represented by explanatory variable(s) in the analysis (in matrix **X**)

F: factor not represented by explanatory variable(s) in the analysis

for community variation. Table 14.1 summarizes the interpretation of the fractions of variation of Fig. 10.10, assuming that matrix **W** contains spatial eigenfunctions. The following examples refer to factors that may intervene to explain community variation in a temperate forest; they illustrate the statements found in Table 14.1.

[a] The environmental and biotic factors that are explicitly represented by variables in matrix  $\mathbf{X}$  and generate the variation explained by fraction [a] have either local effects or spatial variation at scales finer than those detected by the spatial eigenfunction model. Besides these factors, local variation in unobserved soil chemistry data or other environmental variables may affect the community structure (matrix  $\mathbf{Y}$ ) as well as the explanatory variables found in  $\mathbf{X}$ , a case that would lead to covariation between  $\mathbf{X}$  and  $\mathbf{Y}$  (false correlation). In addition, localized infestation by pest insects may have occurred in the past, leaving variation at some sites in the forest that persisted throughout the years; such a historical event may also have left traces in the variables included in  $\mathbf{X}$ , for instance a higher content in soil organic matter due to larger amounts of dead wood deposits, leading to causal or non-causal correlations.

[b] The environmental and biotic factors that are explicitly represented by variables in  $\mathbf{X}$  often have spatial variation, detectable by the spatial eigenfunction model, which may explain part of the variation of the forest community. Besides these factors, spatial variation in unobserved environmental factors may affect the community structure (matrix  $\mathbf{Y}$ ) as well as the explanatory variables found in  $\mathbf{X}$ , a case that would lead to covariation between  $\mathbf{X}$  and  $\mathbf{Y}$  (false correlation). In addition, past occupation of the territory under study by agriculture may have left spatially-structured variation in the forest community; it may also have left traces in the measured soil variables of matrix  $\mathbf{X}$ , leading to causal or non-causal correlations. Spatial correlation in both the response and explanatory variables may cause covariation between matrices  $\mathbf{Y}$  and  $\mathbf{X}$ , hence inflating fraction [b].

[c] Part of the spatial structure of the community may be caused by environmental or biotic factors that were not included in the analysis; for instance, a soil moisture gradient or the effects of grazers may not have been measured. A windstorm may have occurred in the past, creating a clearing in the forest that was later recolonized and has left a detectable broad-scale spatial structure in the forest community. In other types of communities, competition within or among species may play an important role but may have been left unmeasured. Neutral community processes such as growth and reproduction are also a major source of spatial autocorrelation (eq. 1.2), which is responsible for part of the spatially-structured variation observed in communities; it cannot be explained by external factors.

[d] This fraction represents the unexplained variation of matrix  $\mathbf{Y}$  that either is not spatially structured, or has spatial structure at scales finer than those detected by the spatial eigenfunction model. Some of that variation may perhaps be explained by factors that have not been included in the analysis, such as local patches of grazers. If these explanatory variables had been included in  $\mathbf{X}$ , that variation would have contributed to fraction [a]. The remainder is random local variation, which may be referred to as *local innovation*, and sampling error.

The above examples illustrate the fact that, in some cases, trying to increase the fraction of explained variation by incorporating more environmental variables into the model is doomed to failure. Fraction [c], which may represent an important proportion

of the unexplained variation, can often only be explained by neutral population or community-based spatial processes (e.g. reproduction, biotic interactions) or by past events that can sometimes be documented, but remain often unknown to the investigator.

Partitioning the spatial variation of communities into components and mapping them allow researchers to find interesting correlations that are consistent with models of causal relationships. It also allows one to quantify and map fraction [c], which measures by how much preconceived models fall short of accounting for all the spatial variation in data. The same type of analysis can be conducted on time series. Ecologists can use insights obtained by analysing fraction [c] to formulate better ecological hypotheses, which they may undertake to test by going back to the field to collect new data (Borcard & Legendre, 1994; Section 13.5, numerical example).

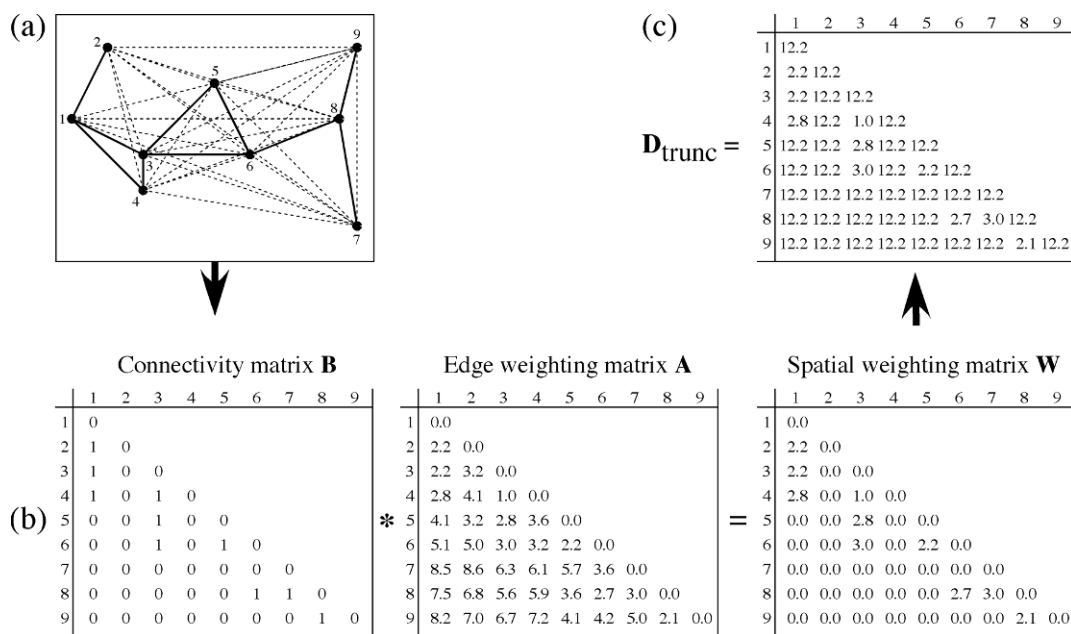
## 14.2 Moran's eigenvector maps (MEM), general form

MEM Dray *et al.* (2006) developed a general algebraic formulation for the construction of *Moran's eigenvector maps*, or MEM eigenfunctions. They observed that the computation of dbMEM (Section 14.1) actually involved two different types of information (Fig. 14.10). The first type is found in connectivity matrix **B**, which contains information about the presence or absence of connections between points. The graph edges representing the connections in Fig. 14.10a are coded in binary form in matrix **B**: the value is 1 if there is a black edge between two points, and 0 otherwise. The second type of information is found in the edge weighting matrix **A**, which contains the values, or weights, that are placed on the edges of the graph. In this generalized approach, matrices **B** and **A** are constructed separately; **B** can contain any type of graph and **A** any type of weights.

### *1 — Algorithm described through an example*

This generalization leads to a new algorithm for the construction of dbMEM eigenfunctions, different from that of Section 14.1.1, which will now be described. Following the description of the new algorithm for dbMEM, Subsection 14.2.2 will explain how to obtain MEM eigenfunctions that differ from dbMEM. In the numerical example that follows (next paragraph), the algorithm is described with *distances* in matrix **A**. In the paragraph after the numerical example, the algorithm is redescribed with *similarities* in matrix **A**.

**Numerical example 3 (continued).** Let us consider again the data (nine points) used in Numerical example 3 of Subsection 14.1.2. These points were used to illustrate different types of connection networks (graphs) in Figs. 13.22 to 13.24. The point coordinates are shown in Fig. 13.22, and Fig. 14.10a displays lines representing the distances among the points.



**Figure 14.10** Generalized MEM eigenfunctions are the principal coordinates of matrix  $\mathbf{D}_{\text{trunc}}$ . (a) Graph of the nine sites of Numerical example 3, drawn on a map. The 10 distances that are equal to or shorter than the longest edge of the minimum spanning tree (Fig. 14.3) are in black, those that will be discarded are represented by dashed grey lines. The largest distance in black in the graph, 3.04, is the *thresh* value. It is found between sites 7 and 8. (b) Connectivity matrix **B** where the 10 edges in black in panel (a) are represented by values 1, the other edges by 0. The weight matrix **A** can contain any set of weights of interest. In this example, it contains the distances among points. Matrix **W** is the result of the Hadamard product (represented by \*) of **B** and **A**. (c) Matrix  $\mathbf{D}_{\text{trunc}}$  is obtained by replacing the zero values in **W** by 4 times *thresh*:  $4 \times 3.04 = 12.16$ , rounded to 12.2 in the figure. The diagonal contains values  $4 \times \text{thresh}$ , indicating that a site is not connected to itself. For clarity, only the lower triangular and diagonal portions of the matrices are represented; all four matrices are symmetric.

- The 10 edges in black in Fig. 14.10a are equal to or shorter than the longest edge of the minimum spanning tree (Fig. 14.3), which has a length of 3.04 units. That value is chosen as the *thresh* value, as in Numerical example 3 of Subsection 14.1.2.

Connectivity matrix **B**

- Construct the binary *connectivity matrix B* (Fig. 14.10b, left). In that matrix, the 10 distances equal to or smaller than *thresh* are represented by 1 (connection edges present) and those larger than *thresh* are coded 0 (no connection).

Edge weighting matrix **A**

- Construct the *edge weighting matrix A* (Fig. 14.10b, centre). The weights can be any set of values that are appropriate for the problem at hand, representing the *difficulty of exchange* between points. In the present example, the inter-point distances are used as weights.



Spatial  
weighting  
matrix **W**

- Compute the Hadamard product (Section 2.5) of **B** and **A** to obtain the *spatial weighting matrix* **W** (Fig. 14.10b, right). The 10 distances in matrix **A** that correspond to edges coded by 1 in **B** are preserved in **W**; the other distances are replaced by zeros. Note that the diagonal contains zeros; these values will be changed in the next step.
- Construct matrix **D<sub>trunc</sub>** (Fig. 14.10c). It is obtained by replacing the zero values in **W** by 4 times the *thresh* value. The fact that the zeros on the diagonal are replaced by  $4 \times \text{thresh}$  indicates that a site is not connected to itself.
- Compute the principal coordinates of matrix **D<sub>trunc</sub>** by PCoA (Section 9.3): they are the MEM eigenfunctions. For the present example where inter-point distances were used in matrix **A**, the MEM eigenfunctions obtained are identical to the dbMEM eigenfunctions of Numerical example 3; they are plotted in Fig. 14.4. This example shows that dbMEM are but a special type of MEM eigenfunctions. Other values than inter-point distances will be used in the next subsection. Because matrix **D<sub>trunc</sub>** has non-zero values on the diagonal, the function used to compute PCoA must not assume that the diagonal contains zeros\*.

In the Dray *et al.* (2006) paper, the algorithm is described in terms of *similarities* instead of distances. To obtain dbMEM eigenfunctions identical to those of Section 14.1, the edge weighting similarity matrix **A** = [ $a_{ij}$ ] is computed as

$$a_{ij} = 1 - \left( \frac{d_{ij}}{4 \times \text{thresh}} \right)^2$$

and the inter-point distances are used as the  $d_{ij}$  values. The  $a_{ij}$  are similarities representing the *ease of communication* of matter, energy or information between points. **A** is multiplied (Hadamard product) with connectivity matrix **B** (where  $b_{ij} = 1$  when  $d_{ij} \leq \text{thresh}$ ) to produce **W**, which contains zeros for all excluded distances. The diagonal elements are also zero, indicating that a site is not similar, or connected, to itself. This is still a similarity matrix since, among the non-zero entries, larger values indicate more strongly connected pairs of points. Matrix **W** is subjected to PCoA computed for a similarity matrix, as described in Subsection 9.3.3. The computation steps are the following: (1) skip eq. 9.40, (2) centre the similarity matrix (eq. 9.41 or 9.42), and (3) proceed with eigen-decomposition of the centred matrix. The eigenvalues are the same as those computed from **D<sub>trunc</sub>** in the previous paragraph, to within a multiplicative constant. The eigenvectors normalized to 1 are identical to those of the previous paragraph when they are also normalized to 1. They are the dbMEM eigenfunctions.

MEM eigenfunctions with positive eigenvalues are usually presented scaled to lengths of  $\sqrt{\lambda_k}$  since they are the result of principal coordinate analysis. MEM with

---

\* The computation of principal coordinates analysis for matrices with non-zero diagonals is available in function *pcoa.all()* of package PCNM (Section 14.7). That function also contains an option that allows users to output the principal coordinates corresponding to negative eigenvalues. These eigenvectors are outputted as they are computed by function *eigen()*, i.e. normalized to lengths of 1. They are not scaled to lengths of  $\sqrt{\lambda_k}$ .

negative eigenvalues must be presented scaled to lengths of 1, however, because scaling them to lengths of  $\sqrt{\lambda_k}$  would produce complex vectors in which each value would have a real and an imaginary part. When they are used as explanatory variables in regression or canonical analysis, including variation partitioning, eigenfunctions scaled to any value have the same explanatory power and produce the exact same  $R^2$ . This is why scaling them to lengths of 1 instead of  $\sqrt{\lambda_k}$  is legitimate in MEM analysis, where the eigenfunctions are used as explanatory variables in regression or canonical analysis.

## 2 — Different types of MEM eigenfunctions

Graph  
Nodes,  
edges

In spatial/landscape studies in ecology, study sites can be depicted as linked by different types of relationships (spatial neighbouring, exchange routes, mutual effects, etc.), which are represented by lines drawn on maps. Landscape analysis is also of interest in genetics, evolution, epidemiology, anthropology, demography, economics, and related fields. *Graphs* are schematic representations of relationships among sites. *Graph theory* is the mathematical study of graphs, which are structures used to model pairwise relations between the objects of interest in a study. In graph theory, the sites are called *nodes* and the lines are called *edges*. Urban *et al.* (2009) and Dale & Fortin (2010) reviewed the use of graphs in ecology. Graph theory was briefly used in Section 8.2.

Spatial,  
aspatial  
graph

Dale & Fortin (2010) explained the difference between aspatial (non-spatial) and spatial graphs. Examples of aspatial graphs are food webs and atoms linked by chemical bonds to form molecules (atom positions in these models are chemical relationships, not measured positions). Among the spatial graphs, the authors distinguished between planar spatial graphs, which are used in the present section to create the binary connectivity matrix **B**, and directed spatial graphs, which will be of interest in Section 14.3. They reviewed the use of graphs in landscape studies in ecology, evolution, genetics, and epidemiology.

Matrix **B** can be constructed using different types of graphs like those described in Subsection 13.3.1 for regular grids or irregularly-spaced points on a map. The present subsection describes how to obtain different types of MEM eigenfunctions by modifying the contents of matrices **B** and **A**, followed by computation of eigenfunctions as explained in Section 14.2.1. The main categories are the following:

Binary  
MEM

1. *Binary MEM eigenfunctions*. — In some problems, only the presence of connections among sites matters. Differentiated values on the edges may be of no interest, or cannot be determined, so that the weights in matrix **A** are all equal. This type of spatial eigenfunctions was developed by statistical geographers; the literature on this subject was reviewed by Tinkler (1972) and Griffith (1996). Griffith & Peres-Neto (2006) called this type of methods *topology-based spatial filtering* because computation of the eigenfunctions is based on the topology of the connection network described by the spatial connectivity matrix **B**. In applications of spatial eigenfunction analysis by Tinkler (1972) and other authors, a transport network composed of

locations (nodes) and routes linking them (edges) was represented by a binary connectivity matrix, and the structure of the network was characterized by the eigenvectors of that matrix, called eigenfunctions. In Griffith (1996), urban census areas that were spatially adjacent were connected in matrix **B** (called **C** by Griffith) and non-adjacent areas were not connected. After centring matrix **B** (eq. 9.41 or 9.42), eigenfunctions were computed; they characterized the spatial relationships among the census areas. In all these applications, inter-point distances were not taken into consideration.

Transformed distances      2. *Transforming the geographic distances recorded in A.* — In some problems, the geographic distance does not produce the best set of explanatory eigenfunctions, and more efficient sets of eigenfunctions are found by using some non-linear function of the geographic distances. Dray *et al.* (2006) proposed three families of functions for nonlinear transformation of the geographic distances into similarities, which are used in the SPACEMAKER package. Different exponent values can be tested in turn to find the transformation of distances that produces the best model for a matrix of response data<sup>\*</sup>.

• Linear function  $f_1$ :

$$s_{ij} = 1 - \frac{d_{ij}}{\max(d_{ij})} \quad (14.2)$$

where  $d_{ij}$  is the geographic distance between points  $i$  and  $j$ . Division by  $\max(d_{ij})$  ensures that the similarities are in the range  $[0, 1]$ .  $f_1$  does not change the modelling capacity of the resulting MEM eigenfunctions: in an analysis based on a matrix  $[d_{ij}' = d_{ij}/\max(d_{ij})]$ , the eigenvalues are changed compared to an analysis based on matrix  $[d_{ij}]$ , but the eigenvectors scaled to lengths 1 are the same.  $f_1$  is presented here as a reference to help in understanding  $f_2$ .

• Concave-down function  $f_2$ :

$$s_{ij} = 1 - \left( \frac{d_{ij}}{\max(d_{ij})} \right)^\alpha \quad (14.3)$$

With  $\alpha > 0$ , function  $f_2$  operates a non-linear transformation of distances  $d_{ij}$ . The similarity  $s_{ij}$  decreases as  $d_{ij}$  increases, but more rapidly for larger  $d_{ij}$  values. When  $\alpha = 1$ ,  $f_2$  is the same as  $f_1$ . To appreciate the shape of the transformation, readers can compute this function for  $d_{ij}$  values from 1 to 20, using a positive integer larger than 1 for  $\alpha$ , and plot the results. Fractional positive values of exponents  $\alpha$  produce concave-up transformations where the similarity  $s_{ij}$  decreases less rapidly for larger  $d_{ij}$  values.

<sup>\*</sup> Function *test.W()* of the SPACEMAKER package allows users to automatically test the effect of different exponents of functions  $f_2$  and  $f_3$ , or any other function that transforms the distances before they are included in matrix **A**, and select the one that produces the model with the lowest value of AIC<sub>c</sub> (eq. 10.23). A tutorial (Dray, 2010) is provided with the package.

- Concave-up function  $f_3$ :

$$s_{ij} = 1/d_{ij}^{\beta} \quad (14.4)$$

where  $\beta$  is a positive real number. The similarity  $s_{ij}$  decreases as  $d_{ij}$  increases, but less rapidly for larger  $d_{ij}$  values.

Other transformations of geographic distances to similarities can be devised and applied to data. In their search for the best predictive model for the oribatid mite data also used in Ecological applications 11.5 and 14.4, Dray *et al.* (2006) tried in turn functions  $f_1$ ,  $f_2$  with  $\alpha = 2$  to 10, and  $f_3$  with  $\beta = 1$  to 10. A similarity matrix  $\mathbf{S}$  was computed for each of these functions and exponent values.  $\mathbf{S}$  was used as the edge weighting matrix  $\mathbf{A}$  to compute the spatial weighting matrix  $\mathbf{W}$ , which was decomposed into MEM eigenfunctions. After selection of the best MEM submodel in each case, the set of MEM eigenfunctions that produced the lowest value of  $AIC_c$  (eq. 10.23) was retained as the best spatial model of the response data. Details are presented in Ecological application 14.2a hereunder.

When  $f_1$  or  $f_2$  provides the best predictive model, the following method can be used: compute a minimum spanning tree for matrix  $\mathbf{D} = [1 - s_{ij}]$  to identify the value of *thresh*, then replace  $\max(d_{ij})$  by  $(4 \times \text{thresh})$  in the denominators of transformation equations  $f_1$  and  $f_2$ ; for example,  $f_1: s_{ij} = 1 - (d_{ij}/(4 \times \text{thresh}))$ . This alternative method, which uses *thresh*, would be in line with the similarity-based procedure for dbMEM described in Subsection 14.2.1.

Geographic  
resistance

3. *Using other measures of geographic resistance as weights in A.* — The edge weighting matrix  $\mathbf{A}$  can be generalized further by using measures of landscape resistance that are not based on transformations of the geographic distances. Dale & Fortin (2010) give several examples. One of them is the analysis of animal movement, which can be based on estimates of the attractiveness of patches for the species under study, or on estimates of movements obtained from field observations. Other aspects that can be used to construct matrix  $\mathbf{A}$  are transport models, landscape connectivity, least-cost paths, and multiple paths forming corridors. Applications of these measures of resistance in landscape ecology and genetics have yet to be fully explored.

The MEM eigenfunctions obtained in these different ways can all be grouped into spatial submodels corresponding to different spatial scales, which can be analysed by RDA, mapped, and interpreted separately. Dray *et al.* (2006) remind users that the choice of a spatial weighting matrix  $\mathbf{W}$  in the similarity approach, or  $\mathbf{D}_{\text{trunc}}$  in the distance-based approach, is a critical step in spatial eigenfunction analysis. While the structures modelled by eigenfunctions obtained using different  $\mathbf{A}$  matrices are fairly similar for regular sampling designs like regular grids, they may differ greatly for irregular distributions of sites. The authors recommend a pragmatic approach where several solutions are explored and the one that explains the response data best is retained, unless ecological theory suggests a specific way for the construction of  $\mathbf{A}$ , e.g. knowledge of propagule dispersal processes. In linear modelling, model efficiency can be estimated by the  $AIC_c$  coefficient (eq. 10.23) associated with the model.

### Ecological application 14.2a

An example of MEM analysis with selection of the geographic distances leading to the best model is included in the Dray (2010) tutorial document about MEM eigenfunction analysis. It was reproduced, with additional comments, in Borcard *et al.* (2011, Subsection 7.4.3.2). The application involves the oribatid mite data already used in Ecological application 11.5. In the present application, the detrended and Hellinger-transformed abundances of the 35 mite morphospecies were used together with the spatial coordinates of the 70 soil cores from which the mites were extracted. Geographic distances were computed among the core positions. For reference, dbMEM analysis (Subsection 14.1) of the same data produced a spatial model containing eight MEM eigenfunctions that explained the mite data with  $R_a^2 = 0.24$ . Can one find a better spatial model of the mite data?

The first attempt was based on a Delaunay triangulation with binary weights (1 for presence of an edge, otherwise 0) in the edge weighting matrix **A**. Forward selection of MEM eigenfunctions was carried out by function *ortho.AIC()* of the SPACEMAKER package (Section 14.7). That function computes  $AIC_c$  for successive models containing orthogonal explanatory variables ordered by their contributions to  $R^2$ . The best model, i.e. the one with the lowest  $AIC_c$ , contained seven MEM variables. Its  $AIC_c$  value was  $-94.2$ .

In an attempt to find a better model, the edges of the Delaunay triangulation were weighted using function  $f_2$  described above. Values of exponent  $\alpha$  from 1 to 10 were investigated ( $f_2$  with  $\alpha = 1$  is function  $f_1$ ), and for each exponent, forward selection was performed. The best among these models turned out to be one obtained with  $\alpha = 1$ . The value of  $AIC_c$  was  $-95.5$ , lower than with binary weights; the model contained six MEM variables.

In a further attempt to find a better model, connectivity matrices **B** were constructed based on inclusion circles of increasing radii around each point. A multivariate variogram (Subsection 13.1.4) showed that spatial correlation was maximum at a distance of about 4 m. Since the shortest distance that kept all points connected in a minimum spanning tree was  $thresh = 1.01$  m, the distances to be investigated covered the range [1.01 m, 4 m]. Ten circle sizes were created. For each value, the inter-point distances smaller than or equal to the stated distance value were coded by 1 in matrix **B**. There were no weights in matrix **A**. The connection network with distances smaller than or equal to 2.01 produced the best model; it had an  $AIC_c$  coefficient of  $-100.6$ . The model contained five MEM variables.

The search for the best model was broadened by combining different distance thresholds, as in the previous paragraph, with weighting the edges in matrix **A** using function  $f_2$  with different values of exponent  $\alpha$ . The connection network with distances  $\leq 2.67$  produced the best model when combined with exponent  $\alpha = 3$ . That model had  $AIC_c = -102.7$ ; it included seven MEM eigenfunctions.

The  $R_a^2$  statistic increased along that search. It was 0.20 for the two models based on Delaunay triangulations, 0.21 for the model that included all distances  $\leq 2.01$  but no weights, and 0.29 for the model that included all distances  $\leq 2.67$  weighted by  $f_2$  with exponent  $\alpha = 3$ . That last model, which involved seven MEM eigenfunctions, led to a RDA that produced two significant axes representing two orthogonal spatial models, whose values can be plotted on maps of the 70 soil cores, as suggested in the R script provided by Borcard *et al.* (2011). Careful empirical selection of the spatial weighting matrix **W** produced a much better model, in terms of  $AIC_c$  and  $R_a^2$ , than the initial model. The final model is parsimonious in terms of the number of MEM eigenfunctions that are included.

## Ecological application 14.2b

Landeiro *et al.* (2011) compared MEM eigenfunctions derived from geographic distances and from distances along a river network, called watercourse distances, in an ecological study of a stream network in the Ducke Reserve in Central Amazon, Brazil. The eigenfunctions derived from watercourse distances provided stronger explanations (higher  $R_a^2$ ) of community variation among sampling sites located along the network than eigenfunctions derived from geographic distances, for both real (fish, caddisfly) and simulated data.

### 14.3 Asymmetric eigenvector maps (AEM)

In fluid ecosystems (water, air), distributions of the organisms that form communities are often driven in part by directional physical processes. These include water currents in rivers, lakes and oceans, prevailing wind along mountainsides, river networks, and glaciations at historical time scales. Spatial modelling by MEM eigenfunctions was not designed to take into account such directional processes. A different type of spatial eigenfunction analysis, called *asymmetric eigenvector maps* (AEM), was developed by Blanchet *et al.* (2008a, 2009) to model this type of phenomenon.

#### 1 — Algorithm described through an example

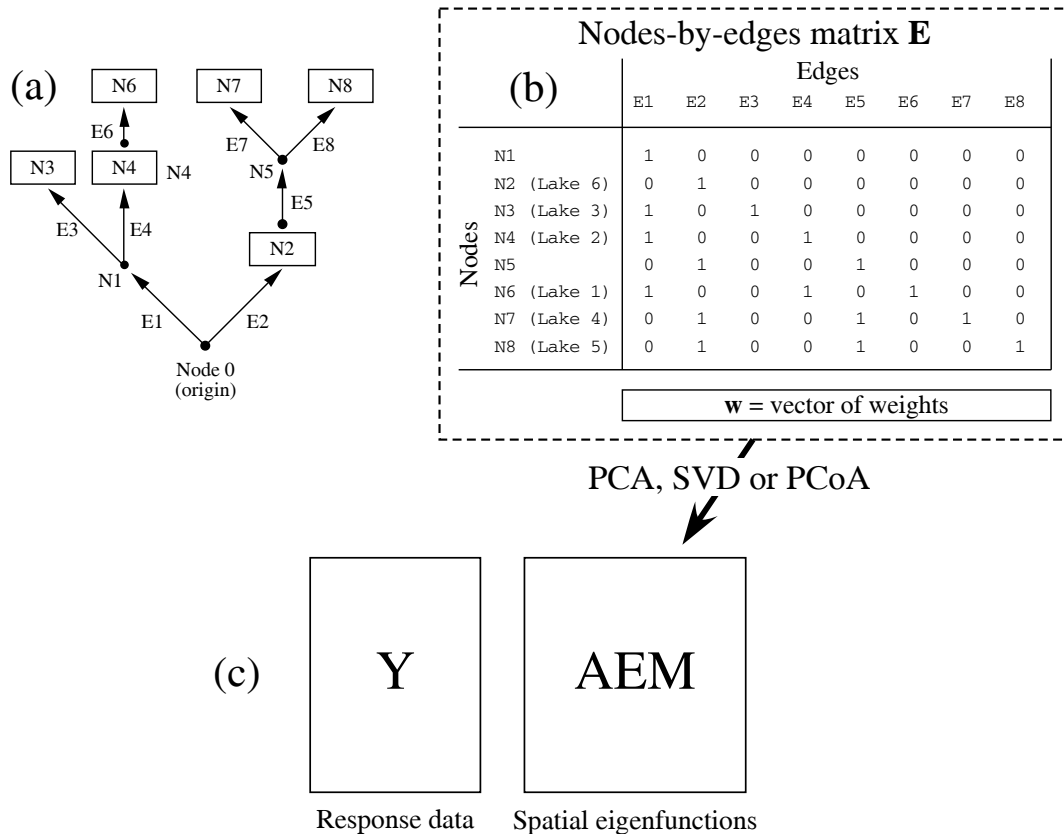
The algorithm for the construction of AEM eigenfunctions representing directional physical processes is described here through an example.

**Numerical example 4.** Let us consider the river network shown in Fig. 14.11a, the same as in Fig. 1.14. The network contains eight nodes (N1 to N8); six of them are lakes, the other two are river junction points. For the sake of the example, let us assume that sampling has taken place at these eight nodes. One could study fish communities found either in the six lakes, or at all nodes. Even if no data are available at the root of the network, a non-sampled node 0 is added there to unite the network into a single structure. AEM modelling could be used to test the hypothesis that the communities are spatially related through a process of colonization of the network from node 0.

The river network can be coded as shown in Fig. 14.11b:

Nodes-  
by-edges  
matrix

- The nodes are the rows of the coding table (matrix **E**), the columns are the edges. In matrix **E**, an edge located between node  $i$  and node 0 is coded 1 in the row corresponding to node  $i$ ; the other edges are coded 0. The coding is the same as in Fig. 1.14. For a denser connection network, as in Fig. 1 of Blanchet *et al.* (2009), matrix **E** can often have many more columns than rows.
- A vector of weights  $\mathbf{w} = [w_j]$  may be applied to the edges. The weights may be based upon geographic distances, estimates from a flow model, current speed, and so on. They represent the ease of communication of matter, energy or information among the sites. The weight values must be structured as similarities between nodes, not as distances, so that larger weights produce higher values in the matrix  $\mathbf{E}_w$  resulting from the scalar product of **E** by the diagonal matrix of



**Figure 14.11** Schematic of AEM analysis. (a) River network from Fig. 1.14. The  $N_i$  are nodes and the  $E_j$  are edges. The nodes in boxes are lakes, labelled Lake 1 to Lake 6 in Fig. 1.14. The node at the origin of the network is labelled Node 0. (b) Nodes-by-edges matrix  $\mathbf{E}$ . PCA of matrix  $\mathbf{E}$  or  $\mathbf{E}_w$  (weighted), or SVD of  $\mathbf{E}_c$  (centred) or  $\mathbf{E}_{wc}$  (weighted and centred), or PCoA of a distance matrix computed from  $\mathbf{E}$  or  $\mathbf{E}_w$ , produces the table of AEM spatial eigenfunctions, which is used in (c) to analyse the variation of response matrix  $\mathbf{Y}$  by RDA.

weights  $\mathbf{D}(w_j)$ . Matrix  $\mathbf{E}_w$  has the same number of rows and columns as  $\mathbf{E}$ . The initially chosen weights may be reworked through weighting functions  $f_1, f_2$  and  $f_3$  of Subsection 14.2.2 in order to transform them in an optimal way. Several examples of the search for optimal weights are found in the applications presented by Blanchet *et al.* (2011).

The weighted or unweighted matrix,  $\mathbf{E}_w$  or  $\mathbf{E}$ , is subjected to principal component analysis (PCA); matrices  $\mathbf{F}$  or  $\mathbf{G}$  of the PCA output contain the AEM eigenfunctions. Alternatively, matrix  $\mathbf{E}$  can be centred by columns, producing  $\mathbf{E}_c$ , and then subjected to singular value decomposition (SVD). A third computational approach is to compute a Euclidean distance matrix ( $D_1$ , eq. 7.32) among the rows of  $\mathbf{E}_w$  or  $\mathbf{E}$ , followed by principal coordinate analysis

(PCoA, Section 9.3). The three forms of decomposition produce equivalent AEM spatial eigenfunctions.

PCA produces matrices **F** or **G** of object scores (eqs. 9.4 and 9.14), SVD produces matrix **V** (eq. 2.31), and PCoA produces a matrix of eigenvectors rescaled as principal coordinates. All four matrices can be used interchangeably as the explanatory matrix in the next step of the analysis because they only differ by the scaling of their vectors. The singular values obtained by SVD can be transformed into the eigenvalues of the PCA, as shown in Subsection 9.1.9; the relationship between the eigenvalues of the PCoA of a Euclidean distance matrix ( $D_1$ ) and those of the PCA computed on the same original data has been shown in Subsection 9.3.2. Contrary to MEM where positive and negative eigenvalues are found, all AEM eigenvalues are positive or null because PCA eigenvalues cannot be negative (Section 9.1).

Contrary to MEM analysis, the response data should not be detrended (Subsection 13.2.1) prior to AEM analysis. The reason is that a gradient structure is a logical consequence of a directional forcing process, and detrending would remove a portion of its expected signature. This makes the comparison of the results of MEM and AEM modelling difficult. An example in Blanchet *et al.* (2011) shows how to resolve that problem by introducing a model corresponding to the spatial trend in the variation partitioning operation involving the MEM and AEM models.

For the example, if response data (e.g. fish community composition) were only available for the six lakes, the rows of **E** corresponding to the six lakes could be selected for PCA, SVD or PCoA instead of the whole matrix **E**. The number of columns would remain the same, although columns containing only zeros, if present, could be discarded before decomposition since they would have no effect on the AEM eigenfunctions.

The matrix of AEM eigenfunctions can now be used as explanatory data in multiple regression analysis to explain the variation of univariate response data **y**, or in RDA to explain the variation of multivariate response data **Y** (Fig. 14.11c).

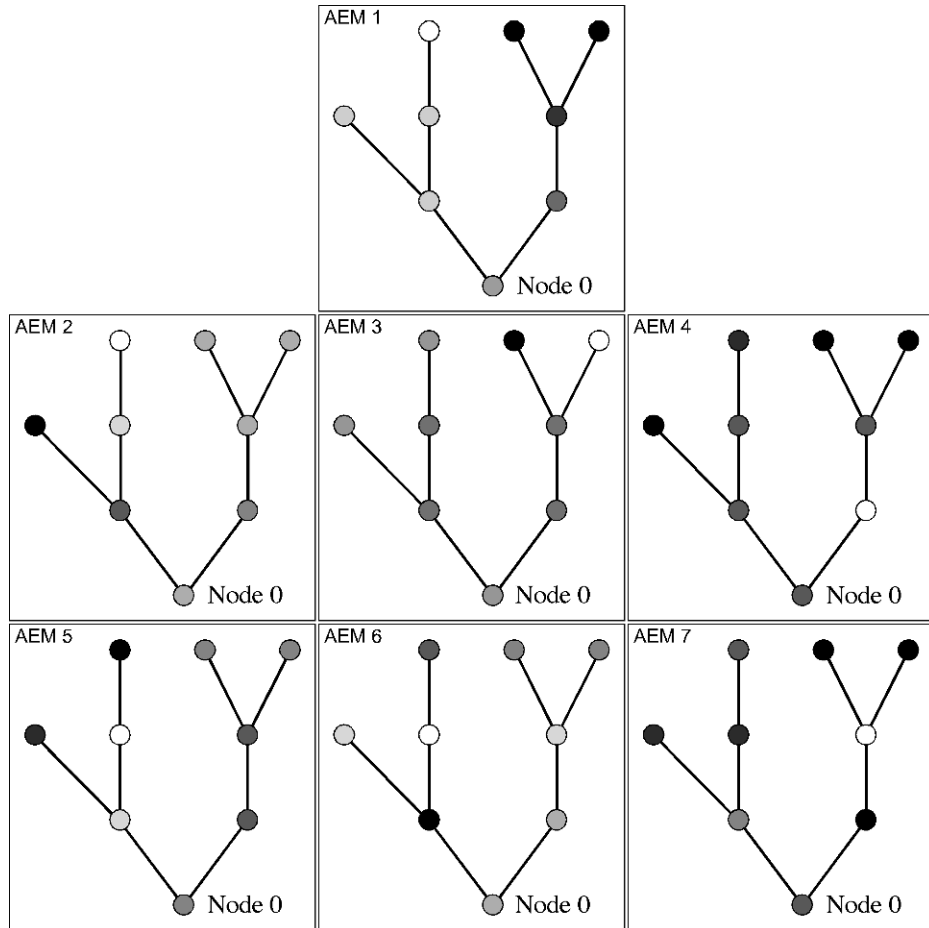
Moran's *I* coefficients (eq. 13.1) can be computed for each AEM eigenfunction\* (Blanchet *et al.*, 2011); this allows users to separate the eigenfunctions modelling positive and negative spatial correlation, and select one of the two groups for analysis. The eigenfunctions of the selected group can then be divided into submodels for multiscale analysis. The whole matrix of AEM, or the submodels, can be used jointly with other matrices of explanatory variables in variation partitioning. The latter form of analysis may involve environmental explanatory data. It can also involve MEM eigenfunctions, which model non-directional spatial processes; an example is found in Ecological application 14.1a. Before variation partitioning, a hierarchy can be established among the AEM submodels to avoid the production of un-interpretable non-zero fractions of shared variation between the orthogonal submodels; else, the intersection fractions can be apportioned proportionally to the variation explained by each submodel (Legendre *et al.*, 2012); see Fig. 14.7b.

For the example (Fig. 14.11), AEM eigenfunctions were computed with edges having equal weights of 1, i.e. all  $w_j = 1$ . The first four eigenfunctions had Moran's *I* larger than the expected value  $E(I)$  and thus modelled positive spatial correlation. Bubble maps are shown in Fig. 14.12;

---

\* Moran's *I* coefficients can be computed using function *moran.I.multi()* of the AEM package; see Section 14.7.





**Figure 14.12** Bubble maps of the seven AEM eigenfunctions corresponding to the example in Fig. 14.11. Shades of grey: see Fig. 14.2.

the eight nodes are drawn on top of the river network. AEM 1 displays a double gradient showing the directional process corresponding to the structure of the river network: node shades go from gray (node 0) to white in the left branch and from gray to black in the right branch. AEM 2 differentiates the extreme nodes of the left branch, black versus white; the nodes of the right branch are near the mean value (0, gray) for this AEM. In a similar way, AEM 3 differentiates the extreme nodes of the right branch, black versus white; all the other nodes are zero (gray) for this AEM. AEM 4 displays a concave-up shape with low values near the origin of the network and high values at the tips: the white dot (N2) has the lowest value and from that point, values increase in the right branch to maximum at N7 and N8, and similarly in the left branch to an intermediate value at N6 and a maximum value at N3. The last three AEMs, 5, 6 and 7, show quick successions of black and white dots in the left or right branch; they model

negative spatial correlation on the river network, as shown by their Moran's  $I$  smaller than  $E(I)$ . This set of AEM eigenfunctions is well suited to model directional processes along the network with differentiation of the two main branches.

**Time series** Time series represent a form of directional stochastic process (Section 12.0). To emphasize the directional nature of the process influencing the data, AEM analysis, which was designed to take trends into account, should be applied to the non-detrended series. MEM analysis can be applied to data series that were detrended to remove the directional component (recommendation of Subsection 14.1.2). Detrended palaeoecological sediment core data, for example, could be studied by MEM analysis.

## 2 — Ecological applications

Three applications of AEM analysis drawn from the ecological literature are summarized hereunder.

### Ecological application 14.3a

A fully developed ecological application of AEM analysis is presented by Blanchet *et al.* (2008a). It concerns the diet composition of brook trout, *Salvelinus fontinalis*, collected in 42 lakes in the river network of the Mastigouche Reserve in Québec, Canada. The diet composition of 20 trouts per lake was divided into nine functional prey categories. The data were analysed to test the hypothesis that diet composition was determined at least in part by the structure of the river network, which captured the geomorphological differences among the lakes in different portions of the river network as well as genetic differences among the trout populations, which migrated from lake to lake along the network.

The spatial modelling was conducted in different ways: (1) based on the lake geographic coordinates (polynomial of the coordinates, dbMEM analysis); (2) using the same coding of the nodes as in Magnan *et al.* (1994; coding briefly described in Subsection 1.5.7); and (3) using a coding of the edges as described in Fig. 14.11. Then, the edges of the network were analysed in three different ways: (3.1) RDA with forward selection was conducted on the nodes-by-edges matrix (matrix **E** in Fig. 14.11); (3.2) the edges were used to compute distances along the river network (watercourse distances), assuming that all edges had the same resistance value along the network, and these distances were transformed into MEM eigenfunctions which were used in RDA with forward selection; (3.3) the edges coded into matrix **E** were used to compute AEM eigenfunctions, assuming again that all edges had the same  $w_j$  values, and the AEMs were used in RDA with forward selection.

The analyses based on edges outperformed the analyses based on geographic coordinates of the lakes and on nodes of the network in terms of  $R_a^2$ . The non-directional MEM model based on watercourse distances produced  $R_a^2 = 0.56$  whereas the directional AEM model had  $R_a^2 = 0.64$ . For these data, all the spatial variation explained by the MEM model was also explained by the AEM model, and the latter explained a small but significant extra fraction of variation ( $R_a^2 = 0.08$ ) that was not explained by the symmetric MEM model\*.

---

\* This additional result was computed and provided by F. Guillaume Blanchet, University of Alberta, Edmonton. It is not found in the Blanchet *et al.* (2008a) paper.

Three other application of AEM analysis are found in Blanchet *et al.* (2011). The applications include the distribution of a crustacean (*Atya*) in a river, bacterial production in a fluvial lake, and the distribution of the copepodite stages of a crustacean on the Atlantic Ocean shelf. In each of these applications, the AEM, MEM, and dbMEM modelling results were compared. These applications show that AEM and MEM analyses can often be used together to identify the directional and non-directional components in the spatial structure of ecological data; the overlap between the fractions of explained variation by the two models is often high.

### Ecological application 14.3b

Gray & Arnott (2011) studied zooplankton dispersal among 45 lakes in the Killarney Provincial Park, Ontario, Canada, that were heavily impacted by acidification before and during the 1970's. Zooplankton data were available for 1972, 1990 and 2005.

Spatial modelling and variation partitioning were carried out to determine the relative importance of spatial relationships and environmental control in models explaining the variation in zooplankton community structure over the 45 lakes. The objective was to determine if dispersal was an important determinant of the structure of recovering zooplankton communities over time. Three spatial models were compared: a non-directional spatial dbMEM model based on overland distances, a stream dispersal MEM model using watercourse distances among lakes (as in Ecological application 14.2b), and asymmetric AEM models describing overland dispersal by wind among lakes in the predominant spring and summer wind direction. The analysis was applied to data collected in 1972 (acidified) and in 1990 and 2005 (recovery period).

Analysis of the community structure across the 45 lakes was carried out for the three study periods separately with respect to environmental (physical and chemical) data and the three spatial models, for a total of nine variation partitioning results. The environmental variables had greater effect on zooplankton community structure than the spatial models, yet these had significant effects. In 1972 (highly acidified lakes), the symmetric spatial model had greater effect than the stream dispersal and directional models, but during the following study periods (chemical recovery), the effect of the directional (wind-driven) dispersal model grew and, in 2005, it explained more of the community variation than the symmetric and stream dispersal models. The directional model explained a new portion of the community variation that was not shared with the environmental variables and was larger than that explained by the other two models. The authors concluded that limitation of zooplankton dispersal was an important obstacle to lake recovery after acidification.

### Ecological application 14.3c

Sharma *et al.* (2011) assembled a database on fish community composition (100 species), lake morphology, water quality, climatic conditions, and hydrological connectivity for 9885 lakes in Ontario, Canada. The authors compared dbMEM and AEM models through variation partitioning to determine if the spatial patterns could have been produced by human-mediated or natural modes of dispersal. Examination of the relative roles of spatial structure and environmental conditions showed that most of the explained variation of native species assemblages was governed by environmental conditions. Non-native fish assemblage composition could be related to human-mediated dispersal, showing that the ecological processes that underlaid biogeographical patterns differed for native and non-native fish species.

## 14.4 Multiscale ordination (MSO)

Are the environmental variables responsible for the spatial correlation observed in the response matrix, for example in community composition data? If so, at which distance classes is that effect important? Is it for all scales (distance classes) or for some scales only? Wagner (2003, 2004) addressed these important questions by combining multivariate variograms (Subsection 13.1.4) with simple (Chapter 9) or canonical ordination (Chapter 11), in a form of analysis called *multiscale ordination* (MSO). MSO had originally been described by Noy-Meir & Anderson (1971) and Ver Hoef & Glenn-Lewin (1989) for the analysis of the covariation among species in blocks of different sizes. That form of analysis required a continuous sampling design composed of adjacent or regularly-spaced quadrats along a transect or on a lattice. Wagner (2003, 2004) generalized the method to regular or irregular sampling designs using the geostatistical framework. Spatial eigenfunctions can be incorporated as covariables into MSO; an ecological application will illustrate the interest of doing that.

Wagner's multiscale ordination, described in the present section, is based on multivariate variograms (Subsection 13.1.4) and on ordination methods. It can be carried out using PCA, CA, RDA, CCA, or the partial versions of RDA and CCA. The variables in the multivariate data matrix  $\mathbf{Y}$  must all have the same physical dimensions. If they do not, they need to be standardized before MSO based on PCA or RDA (Subsection 9.1.5) because the variances of individual variables must be summed to obtain the variogram statistics (Subsection 13.1.4); in any case, the condition of dimensional homogeneity of the variables must also be fulfilled before computing PCA or RDA (Subsection 9.1.5). The data used in CA and CCA are frequencies (Section 9.2), which should not be standardized. In the context of simple ordination (PCA, CA), MSO partitions the variance of the ordination axes among distance classes. This exploratory analysis aims at identifying the ordination axes that display spatial structure and finding out if the spatial structure differs among axes. With the canonical ordination methods, the analysis can incorporate matrices of environmental variables and eigenfunctions (MEM or AEM), which makes it possible to determine if the spatial correlation in the data is due to induced spatial dependence (eq. 1.1, Chapter 1) or the presence of spatial autocorrelation in the response data (eq. 1.2).

In the present section, the different levels of analysis will be described for ordination methods of increasing complexity that preserve the Euclidean distance: PCA, RDA and partial RDA. Couteron & Ollier (2005) give details for methods that preserve the chi-square distance (CA, CCA, partial CCA). MSO with Euclidean-based methods is presented in detail here because these methods are flexible; by applying the transformations of Section 7.7 to community composition data, MSO through PCA and RDA can preserve a variety of distances, including the chi-square.

MSO can be computed on non-stationary data (see Ecological application 14.4), but one must be aware of the fact that the calculation of confidence intervals in variograms requires stationarity, a problem that can be solved by detrending the data

(Subsection 13.2.1). With non-stationary data, the confidence intervals are too broad and thus the tests for spatial correlation are too conservative.

The MSO algorithm is implemented as follows in Wagner's function *mso()* of the VEGAN package in R.

1. *MSO with simple ordination (PCA)*. — Consider a multivariate matrix  $\mathbf{Y}$  with  $n$  rows (sites) and  $p$  columns (e.g. Hellinger-transformed species presence-absence or abundance data). The spatial coordinates of the sites along the transect or on the surface must also be provided to the function for the calculation of the distance classes.

- Compute the variogram matrix of  $\mathbf{Y}$  and draw a multivariate variogram, as explained in Subsection 13.1.4. The variogram will indicate the presence of spatial correlation in  $\mathbf{Y}$ , if any, pointing out the distance classes where spatial correlation is significant.
- Compute a PCA of  $\mathbf{Y}$ ; it produces eigenvalues  $\lambda_k$  and eigenvectors  $\mathbf{u}_k$ . Eigenvalue  $\lambda_k$  can be partitioned among distance classes  $d$  by computing  $\lambda_k(d) = \mathbf{u}_k' \mathbf{C}(d) \mathbf{u}_k$  for each distance class. A plot of  $\lambda_k(d)$  against distances  $d$  is a variogram of PCA axis  $k$ . It shows the spatial correlation structure of the variation represented by that axis.

After a PCA, function *mso()* only produces a multivariate variogram of  $\mathbf{Y}$ . The variogram of PCA axes is not presently computed by function *mso()*. One can use a regular univariate variogram function (Section 13.6) to compute a variogram of the  $k^{\text{th}}$  principal component, which is found in matrix  $\mathbf{F}$  of the PCA results (eq. 9.4).

2. *MSO with canonical ordination (RDA)*. — If the multivariate variogram indicates significant spatial correlation, one may test the hypothesis that explanatory (e.g. environmental) data can explain that spatial structure. When it is the case, the spatial structure can be attributed to induced spatial dependence (eq. 1.1). That point can be addressed by MSO based on canonical ordination, using an explanatory matrix  $\mathbf{X}$  to model the spatial variation of  $\mathbf{Y}$ .

- Carry out a canonical ordination by RDA to analyse  $\mathbf{Y}$  using explanatory data  $\mathbf{X}$  that are thought (hypothesized) to drive the observed spatial variation.
- Compute a multivariate variogram of matrix  $\hat{\mathbf{Y}}$  shown in Fig. 11.2. The variogram decomposes the *explained variance* of the RDA model among the distance classes. The variogram statistics can be plotted in a graph. For the first analysis carried out in Ecological application 14.4 (below), the variogram statistics decomposing the explained variation into distance classes are represented by circles in Fig. 14.13a.
- Compute a multivariate variogram of the matrix of *residuals* (Fig. 11.2, lower left matrix) as well as the tests significance of the variogram statistics. Plot the variogram statistics in the graph (squares in Fig. 14.13a). Is there significant spatial correlation remaining in the residual data after fitting the explanatory variables? If not, this result indicates that the explanatory variables  $\mathbf{X}$  explain the multiscale spatial structure well. If significant spatial correlation remains in some distance classes, either there are other

explanatory variables (environmental or historical, Subsection 14.1.4) that may explain that variation but were not included in explanatory matrix  $\mathbf{X}$ , or the remaining spatial correlation is true spatial autocorrelation in the data (eq. 1.2).

- Compute a multivariate variogram of  $\mathbf{Y}$  as described in Subsection 13.1.4. Compute the confidence intervals of the variogram statistics using parametric standard errors. Plot these confidence intervals in the graph (two continuous lines in Fig. 14.13a). The confidence intervals are computed under the second-order stationarity assumption (Subsection 13.1.1).
- Add together the variogram statistics of the explained and residual variation. Plot these sums in the graph (crosses in Fig. 14.13a) and compare them to the confidence intervals plotted in the preceding step (previous bullet). The confidence intervals of the variogram of  $\mathbf{Y}$  provide a diagnostic tool: if the empirical variogram of the explained plus residual variation remains entirely within the confidence envelope, this indicates that the linear relationship between  $\mathbf{Y}$  and the explanatory variables does not vary significantly with scale. In the absence of significant spatial correlation in the residuals, values found outside the confidence envelope may indicate that the relationship between  $\mathbf{Y}$  and the explanatory variables is scale-dependent, or that there may be a mismatch between the scale at which the predictors  $\mathbf{X}$  were measured and the scale of the response of  $\mathbf{Y}$  to these factors (Wagner & Fortin, 2005). The roles of the many mechanisms that may be responsible for the mismatch are still poorly understood and should be the subject of further studies, e.g. by numerical simulations.

If one finds indications of scale-dependent relationships, one can look for the cause either through data analysis or by testing specific hypotheses. For example, one could use MEM eigenfunctions to model the response data at different scales, then regress the fitted values or canonical axes on explanatory data  $\mathbf{X}$  in order to identify the source of the spatial correlations. An example of this approach is presented in Ecological application 14.1a. Another approach is to select MEM eigenfunctions that are significantly related to  $\mathbf{Y}$  and use them as covariables in MSO based on partial RDA; see item 3 below. An example is found in the part of Ecological application 14.4 that is illustrated in Fig. 14.13b.

MSO can be computed for non-stationary data, but beware: because the confidence intervals are then too broad, they may not evidence values of the empirical variogram of the explained plus residual variation that lie outside the confidence envelope of the multivariate variogram.

Although the variogram of the explained plus residual variation is not identical to the variogram of  $\mathbf{Y}$ , the weighted sums of the values in these two variograms are equal to the total variance in  $\mathbf{Y}$ . The weights in these sums are the number of pairs of points used to compute the values in each distance class divided by the total number of pairs of points.

3. *MSO with partial canonical ordination (partial RDA)*. — If an explicit MEM or AEM spatial model is available to account for spatial correlation at scales of interest in the study, the MEM or AEM model can be used as matrix of covariables  $\mathbf{W}$  in partial RDA (Subsection 11.1.6).

- Carry out a partial canonical ordination to analyse  $\mathbf{Y}$  using explanatory data  $\mathbf{X}$  and covariables  $\mathbf{W}$ . The analysis must be computed using the first calculation method of Subsection 11.1.6: residuals of both  $\mathbf{Y}$  and  $\mathbf{X}$  are computed with respect to  $\mathbf{W}$ , obtaining  $\mathbf{Y}_{\text{res}|\mathbf{W}}$  and  $\mathbf{X}_{\text{res}|\mathbf{W}}$ , before the canonical analysis of  $\mathbf{Y}_{\text{res}|\mathbf{W}}$  by  $\mathbf{X}_{\text{res}|\mathbf{W}}$ . This is the method used to compute partial RDA in function *rda()* of VEGAN (Table 11.5).
- Compute a multivariate variogram of the *variance explained* by the partial canonical analysis, i.e. the variance of  $\mathbf{Y}_{\text{res}|\mathbf{W}}$  explained by  $\mathbf{X}_{\text{res}|\mathbf{W}}$ . This variogram can be computed either on the matrix of fitted values of that analysis or on the canonical axes (matrix  $\mathbf{Z}$  in Fig. 11.2), with identical results. It decomposes the variance explained by the partial RDA among the distance classes. Plot these values in a graph; they are represented by circles in Fig. 14.13b for Ecological application 14.4.
- Compute a multivariate variogram of the *residual variation* after fitting matrices  $\mathbf{W}$  and  $\mathbf{X}$ ; compute also the tests of significance of the variogram statistics. Plot these values in the graph (squares in Fig. 14.13b). Is there significant spatial correlation remaining in the residual data after fitting the explanatory variables? If not, this indicates that the explanatory matrices  $\mathbf{X}$  and  $\mathbf{W}$  explain the multiscale spatial structure well.
- Compute a multivariate variogram of  $\mathbf{Y}_{\text{res}|\mathbf{W}}$  as described in Subsection 13.1.4 and compute the confidence intervals on that variogram using parametric standard errors. Plot these confidence intervals in the graph (two continuous lines in Fig. 14.13b).
- Add together the variogram statistics of the explained and residual variation. Plot these sums in the graph (crosses in Fig. 14.13b) and compare them to the confidence intervals already plotted. The confidence intervals of the variogram of  $\mathbf{Y}_{\text{res}|\mathbf{W}}$  provide a diagnostic tool: if the empirical variogram of the explained plus residual variation remains entirely within the confidence envelope, this indicates that the linear relationship between  $\mathbf{Y}_{\text{res}|\mathbf{W}}$  and explanatory matrix  $\mathbf{X}_{\text{res}|\mathbf{W}}$  does not vary with scale.

MSO provides diagnostics about the interpretation of spatial correlation at different scales. Under the assumption that all relevant environmental factors have been measured (and measured at the relevant spatial scales), MSO allows researchers to distinguish between induced spatial dependence and true spatial autocorrelation. These assumptions are difficult to check in practice. It also allows users to assess the presence of significant correlation in residuals, as well as the scale-invariance of the species-environment correlation. How to interpret MSO results is illustrated in Ecological application 14.4.

#### Ecological application 14.4

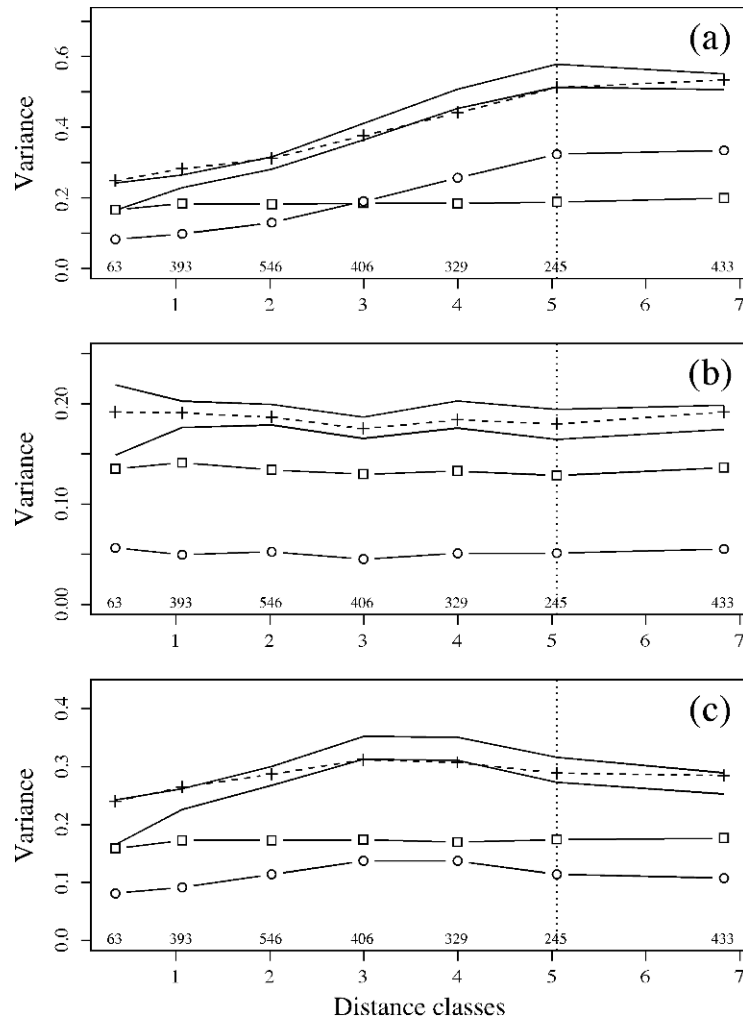
The oribatid mite data of Borcard & Legendre (1994) were used in Ecological application 11.5 to compute a multivariate variogram. The analysis reported here was developed by Borcard *et al.* (2011) to illustrate different facets of MSO analysis. The mite data were Hellinger-transformed prior to analysis. For the variograms, the interval size of the distance classes was the distance that kept all points connected in a dbMEM analysis; this is the threshold distance ( $thresh = 1.0112$  m) computed in Ecological application 14.2a.

In a first set of analyses, a MSO variogram was computed, without detrending, after a RDA of the mite data modelled by several environmental variables. These variables were: substrate density, water content of the soil, substrate types (7 classes), shrub density (3 classes) and microtopography of soil surface (2 classes). The MSO plot is shown in Fig. 14.13a. The confidence interval envelope is that of the multivariate variogram of the Hellinger-transformed mite data, undetrended. Examination of the plot shows that the variogram of the explained plus residual variation (dashed line) increases monotonically, which is the signature of a strong linear gradient in the data. The variogram of the residuals, however, is flat and not significant, showing that the environmental variables account well for the gradient in the data. The dashed line is not within the confidence envelope of the multivariate variogram for distance classes 0, 1 and 4, despite the fact that the confidence intervals, computed using non-stationary data, were too broad. This indicates that the spatial structure of the mite data varied with scale.

In an attempt to determine if a MEM model would successfully control for the spatial structure in the species-environment relationship, MSO was computed from a partial RDA that controlled for a set of seven MEM eigenfunctions selected near the end of Ecological application 14.2a. The results of this second set of analyses are displayed in Fig. 14.13b. The variogram of the explained plus residual variation is now entirely within the confidence envelope of the variogram of  $\mathbf{Y}_{res|W}$  and the separate variograms of explained and residual variation are flat, showing that the MEM eigenfunctions successfully controlled for the spatial correlation of the mite data that was not well explained by the environmental variables. For these data, variation partitioning (Subsections 10.3.5, 11.1.11) showed that the seven selected MEM eigenfunctions accounted almost completely for the linear trend present in both the mite data and the environmental variables. Using the selected MEM as covariables in partial RDA had effectively detrended the mite data as well as the environmental variables because the mite and environmental data were structured by the same spatial trend (Borcard & Legendre, 1994).

In a third series of analyses, the Hellinger-transformed mite data were detrended along the north-south sampling axis to meet the stationarity assumption for the computation of confidence intervals. Will this analysis produce different results than above? A MSO variogram plot was computed after a RDA of the mite data modelled by the same environmental variables as above, except that they were also detrended along the north-south sampling axis, like the mite data. The MSO plot is shown in Fig. 14.13c. The confidence interval envelope is that of the multivariate variogram displayed in Fig. 13.12 where the mite data had also been detrended; the confidence intervals are thus not too broad. The variogram of the explained plus residual variation mostly remains within the confidence envelope, except for distance classes 1, 3 and 4 where a slight departure is observed; this indicates that the species-environment relationship varied slightly with scale. In the variogram of residual variation, none of the statistics forming the variogram are significant, showing that the spatial correlation in the detrended data is well explained by the detrended environmental variables. In summary, the MSO plot indicates that the environmental variables accounted well for the spatial structure in the data although the explained variation shows that the spatial structure varied with scale.





**Figure 14.13** MSO plots of (a) the RDA of the Hellinger-transformed, undetrended mite data, analysed against environmental variables, (b) the partial RDA of the same matrices with MEM eigenfunctions as covariables, and (c) the RDA of the Hellinger-transformed and detrended mite data analysed against detrended environmental variables. Plots produced by function *msor*(). Crosses: variograms of explained plus residual variation. Continuous lines delineate the confidence envelopes of the variograms of  $\mathbf{Y}$  in (a), of  $\mathbf{Y}_{\text{res}|\mathbf{W}}$  in (b), and of detrended  $\mathbf{Y}$  in (c). Squares: variograms of residual variation; the squares are white, indicating that the variogram statistics are not significant in these examples. Circles: variograms of explained variation. Vertical dotted lines: half the maximum number of classes; the last points, to the right of these lines, include all remaining pairs of sites and should not be interpreted. Values written above the abscissas: number of pairs involved in the calculation of each statistic.

As in the second set of analyses, a MSO was computed from a partial RDA that controlled for the seven pre-selected MEM eigenfunctions. The results of this fourth set of analyses were almost identical to those shown in Fig. 14.13b: the variogram of the explained plus residual variation was now entirely within the confidence envelope of the variogram of  $\mathbf{Y}_{\text{resl}}\mathbf{W}$  and the separate variograms of explained and residual variation were flat, showing that the MEM eigenfunctions successfully controlled for the spatial correlation of the detrended mite data that was not well explained by the detrended environmental variables.

The results of this analysis could have differed from Fig. 14.13b if the mite data had been structured by a broad-scale spatial trend running in a different direction from that of the environmental data. Had that been the case, the trend in the undetrended response data  $\mathbf{Y}$  shown in Fig. 14.13b would not be modelled by the undetrended environmental variables  $\mathbf{X}$ . However, the fourth set of analyses described in the previous paragraph, with  $\mathbf{Y}$  and  $\mathbf{X}$  having been both detrended, would not have been impaired by these differing trends.

The R code to run the MSO analyses reported in the present ecological application is found in Section 7.5.3 of Borcard *et al.* (2011).

## 14.5 Other eigenfunction-based methods of spatial analysis

This section describes additional statistical methods based on spatial eigenfunctions that were not covered in the previous sections.

### 1 — *Space-time interaction*

A commonly used approach to test hypotheses about natural or man-made environmental changes, including climate change, is to sample portions of ecosystems repeatedly over time. This type of sampling is usually done without replication of sites; in this way, the sampling effort can be spent on maximizing the expanse of space covered by the study. If the sampling sites and times are represented by dummy variables or Helmert contrasts, as in paragraphs 3 and 4 of Subsection 11.1.10, one can use canonical analysis to study the effect of the sites on species composition while controlling for the effect of time, and vice versa. An important limit of this approach is that the interaction between space and time cannot be estimated for lack of replicates. Assessing that interaction is, however, of great interest in such studies because a significant interaction would indicate that the spatial structure of the univariate or multivariate response data has changed through time, and conversely that the temporal variations differed significantly among the sites, thus indicating, for example, the signature of climate change on ecosystems.

Legendre *et al.* (2010) described a statistical method to *analyse the interaction* between the space (S) and time (T) factors in *space-time studies without replication*; the acronym of the method is STI (for *space-time interaction*). The method can be applied to multivariate response data, e.g. ecological community composition, through partial RDA. The method consists in representing the space and/or time factors by spatial and/or temporal eigenfunctions (MEM, Sections 14.1 and 14.2, or AEM,

STI

Section 14.3). It is not necessary to represent both space and time by eigenfunctions: for example, if there are many sites and only a few sampling times, e.g. 2 or 3, spatial relationships may be coded using spatial eigenfunctions and temporal relationships using dummy variables or Helmert contrasts. Coding the space and/or time factors by spatial and/or temporal eigenfunctions requires fewer coding variables than dummy variables or Helmert contrasts. The interaction can be represented by variables obtained by computing the Hadamard product of each eigenfunction that codes for space with each eigenfunction that codes for time. Enough degrees of freedom are saved to correctly estimate the residual fraction of variation and test the significance of the interaction term.

The above paper gives details about the computation method. The R package STI is available to carry out the calculations (Section 14.7). The paper also contains two applications to real species assemblage data: an analysis of Trichoptera (insects, 56 species) emerging from a stream and captured in 22 emergence traps during 100 days, grouped into 10 consecutive 10-day periods, and a study of four surveys conducted between 1982 and 1995 in the Barro Colorado Island permanent forest plot (315 species of trees). Another application is found in Laliberté *et al.* (2009) where tree seedling abundances at 40 sites along a transect in a temperate forest understory, monitored during a 9-year period, were analysed for space-time interaction. The analysis of spatio-temporal data is also discussed in Cressie & Wikle (2011).

## 2 — *Multiscale codependence analysis*

A causal relationship between an explanatory ( $\mathbf{x}$ ) and a response variable ( $\mathbf{y}$ ) across space implies that the two variables are correlated. When the correlation between  $\mathbf{x}$  and  $\mathbf{y}$  is not significant, the causal hypothesis must be abandoned. Conversely, a significant correlation can be interpreted as support of the causal hypothesis that  $\mathbf{x}$  may have an effect on  $\mathbf{y}$ . Given the multiscale nature of ecological processes, one may wonder at which scales  $\mathbf{x}$  is an important predictor of  $\mathbf{y}$ . The same question can be asked about pairs of variables forming a bivariate time series; for simplicity, the presentation here will focus on space.

### MCA

Guénard *et al.* (2010) developed *multiscale codependence analysis* (MCA) to address the above question and test the significance of the correlations between two variables at different spatial scales. The method is based on spatial eigenfunctions, MEM or AEM, which correspond to different and identifiable spatial scales: indeed, a Moran's  $I$  statistic (eq. 13.1) can be computed for each eigenfunction. If the sampling is regular along a transect, eq. 14.1 can be used to determine the wavelengths of the  $k$  eigenfunctions, which are assembled in a matrix called  $\mathbf{W}$ , of size  $n \times k$ . Correlation coefficients are computed between  $\mathbf{y}$  and each of the  $k$  eigenfunctions, and written in a vector  $\mathbf{r}_{\mathbf{y}\mathbf{W}}$  of length  $k$ . Similarly, correlation coefficients are computed between  $\mathbf{x}$  and each of the  $k$  eigenfunctions, and written in a vector  $\mathbf{r}_{\mathbf{x}\mathbf{W}}$ . The Hadamard product of the two vectors,  $\mathbf{r}_{\mathbf{y}\mathbf{W}}$  and  $\mathbf{r}_{\mathbf{x}\mathbf{W}}$ , is the vector of *codependence coefficients*, which reflect the strength of the  $\mathbf{x}$ - $\mathbf{y}$  correlations at the different scales represented by the eigenfunctions in matrix  $\mathbf{W}$ . Each codependence coefficient can be tested for

significance using a  $\tau$  (tau) statistic obtained by computing the product of the  $t$ -statistics associated with the two correlation coefficients. The testing procedure is described in the paper. An R package is available for the calculations (Section 14.7).

In the above paper, the method was applied to model the river habitat of juvenile Atlantic salmon (parr). MCA showed that variables describing substrate composition of the river bed were the most influential predictors of parr abundance at the 0.4 – 4.1 km scales whereas mean channel depth was more influential at the 200 – 300 m scales. This example shows that when properly assessed, the multiscale structuring observed in nature may be used to refine our understanding of natural processes.

### ***3 – Estimating and controlling for spatial structure in modelling***

The examples and applications reported in Sections 14.1 to 14.3 show that spatial eigenfunctions can efficiently model all kinds of spatial structures in data. Can they be used to find a solution to the problem described in Subsection 1.1.2, that spatial correlation inflates the level of type I error in tests of species-environment relationships in regression and canonical analysis?

A species-environment relationship after controlling for spatial structure can be represented by fraction [a] in a Venn diagram (e.g. Figs. 10.10) showing the partitioning of the variation of response data, univariate  $\mathbf{y}$  or multivariate  $\mathbf{Y}$ , with respect to environmental (left circle) and spatial variables (right circle). A real example is shown in Fig. 14.7. Using numerical simulations, Peres-Neto & Legendre (2010) showed that spatial eigenfunctions provided an effective answer to the problem. Firstly, one must determine if the spatial component of  $\mathbf{y}$  or  $\mathbf{Y}$  is significant. This can be done by regression of  $\mathbf{y}$ , or canonical analysis of  $\mathbf{Y}$ , against all MEM spatial predictors, or by univariate (for  $\mathbf{y}$ ) or multivariate (for  $\mathbf{Y}$ ) variogram analysis. Secondly, if the spatial component is significant, one can select a subset of spatial predictors, and use the environmental ( $\mathbf{X}$ ) and the selected spatial predictors (covariables  $\mathbf{W}$ ) in a partial regression (for  $\mathbf{y}$ , Subsection 10.3.5) or partial canonical analysis (for  $\mathbf{Y}$ , Subsection 11.1.6).

For the analysis of community composition data, the authors found that a species-by-species forward selection procedure, described in their paper, was to be preferred to a global, community-based selection. In this method, eigenfunctions are selected for each species independently, and the union of the selected sets is used as the matrix of MEM covariables in canonical analysis. This provides an effective method of control for type I error in the assessment of species-environment relationships. The paper also showed that polynomial regressors (Subsection 13.2.1) did not produce tests of significance with correct levels of type I error.

The Peres-Neto & Legendre (2010) paper provides theoretical support to the effect observed in Ecological application 14.4, that MEM used as covariables in canonical analysis effectively controlled for the spatial correlation observed in the species-environment relationship in the first part of the analysis of the mite data.

## 14.6 Multiscale analysis of beta diversity

The present book is concerned with the analysis of multivariate ecological matrices, with special emphasis on community composition data. The book started with a difficult problem: Section 1.1 explained the origin of spatial structures in ecosystems, and showed that these structures may be generated by two types of processes, i.e. spatial dependence induced by environmental variables (eq. 1.1) and community dynamics that can generate spatial autocorrelation (eq. 1.2). How can one distinguish between these two families of processes? To do so, it is necessary to analyse community variation at multiple scales.

The focus of ecologists on natural communities of organisms stems from the fact that communities are the best response variable available to assess the effects of natural or man-made changes to the natural environment. Ecologists determine effects by studying how the members of natural communities, i.e. the species, react to changes, appraised through an appropriate sampling design. The difficulty of this approach is that species assemblages form multivariate data tables that cannot be analysed using simple univariate statistical methods. In addition, the presence of spatial structures in communities indicates that some processes have been at work that generated these structures. By relating natural communities to hypothesized causal factors, one can determine if changes observed in communities can be related to these assumed causes. In the face of climate changes and other major anthropogenic impacts, species act as dormant spies in ecosystems that ecologists can awaken to test hypotheses about the origins of changes, which is an essential step before remedial actions can be developed.

Biodiversity is a most important property of ecosystems because of its numerous services to humans, including aesthetic services (Section 6.5). The term biodiversity covers different components: taxonomic (most importantly at the species level), phylogenetic, genetic, ecological and cultural. An important aspect is the spatial organization of biodiversity, called beta diversity — the spatial variation of community composition through space. Some beta diversity studies focus on species turnover along well-identified environmental gradients. A more general concept, followed in this book, is the non-directional approach, where spatial variation of communities is studied not along selected gradients but over whole natural ecosystems. In the latter approach, the variance of a community composition matrix is a measure of beta diversity, and it was shown in this book that this variance can be analysed and decomposed using numerical methods that form a crescendo of power and refinement, from the description of multivariate (multi-species) structures in Chapters 8 and 9 to analyses carried out with respect to explanatory (e.g. environmental) variables in Chapter 11.

After developing concepts and methods of spatial analysis in Chapter 13, the present chapter has come back to the question stated in Section 1.1: how can one study the multiscale structure of communities? Methods based on spatial eigenfunctions

provided answers by drawing upon methods studied earlier in the book: distance measures (Chapter 7), principal coordinate analysis (Section 9.3), linear modelling by multiple regression (Section 10.3.3) and redundancy analysis (Section 11.1), variation partitioning (Sections 10.3.5 and 11.1.11), and the concept of scale in spatial patterns (Section 13.0).

There are already several methods available for multiscale ecological analysis, and more will undoubtedly be developed in the future. The spatial eigenfunction basis described in the present chapter is rich in possibilities, and it is left to the imagination of researchers, driven by ecological questions, to continue the development of derived methods. The help of mathematicians and statisticians will be welcome to provide solid mathematical foundations for these methods. These new methods will hopefully allow researchers to detect more clearly the signals arising from natural communities, which can be deciphered as messages from species spies in ecosystems, and used to manage the balance between human societies and the natural environment.

## 14.7 Software

R-language functions are available to compute all methods of analysis described in this chapter.

1. Distance-based Moran's eigenvector maps (dbMEM). — Package VEGAN contains functions *pcnm()* for construction of dbMEM eigenfunctions. Package PCNM, presently available on [https://r-forge.r-project.org/R/?group\\_id=195](https://r-forge.r-project.org/R/?group_id=195), contains functions *PCNM()* and *quickPCNM()* for classical PCNM and dbMEM analysis. Among the functions available with the Borcard *et al.* (2011) book, *create.MEM.model()* allows users to generate a staggered matrix of dbMEM spatial eigenvectors corresponding to several groups of disconnected sites that are analysed together.

2. Moran's eigenvector maps (MEM), general form. — Package SPACEMAKER, presently available on [https://r-forge.r-project.org/R/?group\\_id=195](https://r-forge.r-project.org/R/?group_id=195), contains functions for MEM spatial modelling. In particular, function *test.W()* computes and tests MEM eigenfunctions for various pre-constructed spatial weighting matrices **W** and selects the best spatial model using AIC.

3. Asymmetric eigenvector maps (AEM). — Package AEM, presently available on [https://r-forge.r-project.org/R/?group\\_id=195](https://r-forge.r-project.org/R/?group_id=195), contains functions for AEM spatial modelling.

4. Multiscale ordination (MSO). — Function *mso()* is available in VEGAN for multiscale ordination.

---

5. Other eigenfunction-based methods of spatial analysis. — To study space-time interaction in surveys without replication: package STI is available on Ecological Archives E091-019-S1 ([http://esapubs.org/archive/archive\\_E.htm](http://esapubs.org/archive/archive_E.htm), year 2010) as well as on the Web page <http://sites.google.com/site/miqueldecaceres/software>. Functions *STImodels()* and *quickSTI()* of that package are also found in package PCNM; see paragraph 1 above. Codependence analysis is available in package CODEP.

6. Miscellaneous methods. — Function *geoXY()* of SODA transforms latitude-longitude (LatLon) data to flat Cartesian coordinates. Variation partitioning involving spatial eigenfunction submodels, with hierarchical partitioning or proportional apportioning of the shared fractions of variation, is found in R functions available in a supplement of the Legendre *et al.* (2012) paper, downloadable from the *ESA Ecological Archives* page [http://esapubs.org/archive/archive\\_E.htm](http://esapubs.org/archive/archive_E.htm).

Package ADESPATIAL, presently under development, will contains functions to carry out the analyses described in Sections 14.1 to 14.3 of this chapter.



**Plate 14.1** Historical dynamics (Section 14.1.4). In the ancient Gallic city of *Burdigala* (now Bordeaux, in southwestern France), the Romans built a Gallo-Roman town around 50 BC. At the beginning of the 2nd century AD, an oval-shaped amphitheatre (132 m  $\times$  111 m) was erected on the northwest outskirts of the city. It was later abandoned, probably during the 4th century, when the ancient city decreased in size and the amphitheatre was left out of the new city walls. At the end of the Middle Ages, the monument was progressively dismantled, in particular its western side. At the beginning of the 19th century, the inside of the amphitheatre was divided into lots where upper middle-class houses were built. The only standing portion nowadays is the northwestern porch (upper-right in the picture). The elliptic outline of the amphitheatre, now called Palais-Gallien, has been preserved in the city plan. It is still visible nowadays on aerial photographs of Bordeaux (44°50'52" N, 00°34'59" W). Information kindly provided by David Hourcade, Institut Ausonius (UMR 5607, *Centre national de la recherche scientifique/Université de Bordeaux 3*), France. Photo reproduced with permission of *Institut national de l'information géographique et forestière*, France (©IGN France, flight 1966\_CDP6309\_P\_8000\_5579).